Macromolecules

Article

Cite This: Macromolecules 2017, 50, 8357-8371

pubs.acs.org/Macromolecules

Poly[(arylene ethynylene)-*alt*-(arylene vinylene)]s Based on Anthanthrone and Its Derivatives: Synthesis and Photophysical, Electrochemical, Electroluminescent, and Photovoltaic Properties

Suru Vivian John,[†,‡] Věra Cimrová,*[,§] Christoph Ulbricht,[‡,∥] Veronika Pokorná,[§] Aleš Růžička,[§] Jean-Benoit Giguère,[⊥] Antoine Lafleur-Lambert,[⊥] Jean-François Morin,[⊥] Emmanuel Iwuoha,*[,†] and Daniel Ayuk Mbi Egbe*[,‡,∥]

[†]SensorLab, Department of Chemistry, University of Western Cape, Robert Sobukwe Road, Private Bag X17, Bellville, 7535, Cape Town, South Africa

[‡]Linz Institute for Organic Solar Cells, Johannes Kepler University, Altenbergerstrasse 69, 4040 Linz, Austria

[§]Institute of Macromolecular Chemistry, The Czech Academy of Sciences, Heyrovský Sq. 2, 162 06 Prague 6, Czech Republic

[∥]Institute of Polymeric Materials and Testing, Johannes Kepler University, Altenbergerstrasse 69, 4040 Linz, Austria

[⊥]Department of Chemistry, Faculty of Science and Engineering, Université Laval, Pavillon Alexandre-Vachon, local 1250B Québec, Québec G1 V 0A6, Canada

Supporting Information

ABSTRACT: Anthanthrone and its derivatives are large polycyclic aromatic compounds (PACs) that pose a number of challenges for incorporation into the structure of soluble conjugated polymers. For the first time, this group of PACs was employed as the building blocks for the synthesis of copolymers (**P1**−**P5**) based on poly[(arylene ethynylene)-*alt*-(arylene vinylene)]s backbone (−Ph−C≡C−Anth−C≡C−Ph−CH=CH−Ph−CH=CH−)$_n$. During the synthesis of **P1**−**P5**, different alkyloxy side chains were incorporated in order to tune the properties of the polymers. Of the copolymer series only **P1** (containing anthanthrone and branched 2-ethylhexyloxy side chains on phenylenes), **P2** and **P3** (for which the anthanthrones containing carbonyl groups were converted to anthanthrene containing alkyloxy substituents) were soluble. The photophysical, electrochemical, electroluminescent and photovoltaic properties of **P1**−**P3** are reported, compared and discussed with respect to the effects of side chains.

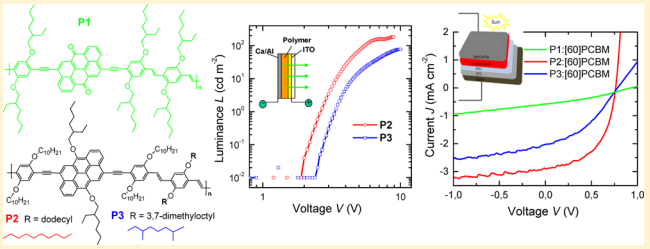

INTRODUCTION

Polycyclic aromatic compounds (PACs) have attracted considerable attention as materials with potential applications in supramolecular electronics[1−3] and are becoming increasingly popular for optoelectronic applications.[4−9] The extensive conjugated π-systems of PACs facilitate electron delocalization, while the rigid flat geometry enables them to stack in well-organized arrays for strong π-stacking interactions. The π-conjugated systems influence the tuning of the optoelectronic properties, while the flat geometry enables good light emitting properties and intermolecular charge transport.[10−15] These combined features make PACs appealing building blocks for the preparation of semiconducting polymers. In spite of this, a comparatively low number of conjugated polymers incorporating large PACs building blocks have been reported so far.[16−24] The low interest in PAC based polymers (especially for organic photovoltaic cells) is as a result of their relatively high band gap. Although the extension of the effective conjugation of the polymers can be used to overcome this drawback,[24−26] it is often accompanied by a significant decrease in solubility, which may hinder their processing into thin films for photovoltaic applications. For example, large hexabenzocoronene PAC was incorporated in the main chain of conjugated polymers.[27] These materials, however, were insoluble in common organic solvents and difficult to process. The synthesis of π-conjugated small molecules based on anthanthrone[28] is relatively simple, but the preparation of their polymeric analogues is challenging. Its rigidity coupled with its large and flat π surface hinders good solubility in common organic solvents. Only very recently, the synthesis and characterization of the first series of soluble conjugated polymers based on anthanthrone derivative (anthanthrene)[29] and 4,10-bis(thiophen-2-yl)anthanthrone (TANT) were reported.[30]

Herein we report for the first time the preparation of poly[(arylene ethynylene)-*alt*-(arylene vinylene)]s (PAE-AVs) from anthanthrone and anthanthrene building blocks, respectively, using the Horner-Wadsworth-Emmons (HWE) polycondensation reaction (Scheme 1).

Received: October 3, 2017
Revised: October 22, 2017
Published: November 3, 2017

DOI: 10.1021/acs.macromol.7b02136
Macromolecules 2017, 50, 8357−8371

Scheme 1. Reaction Pathway for the Synthesis of the PAE-AVs Polymers

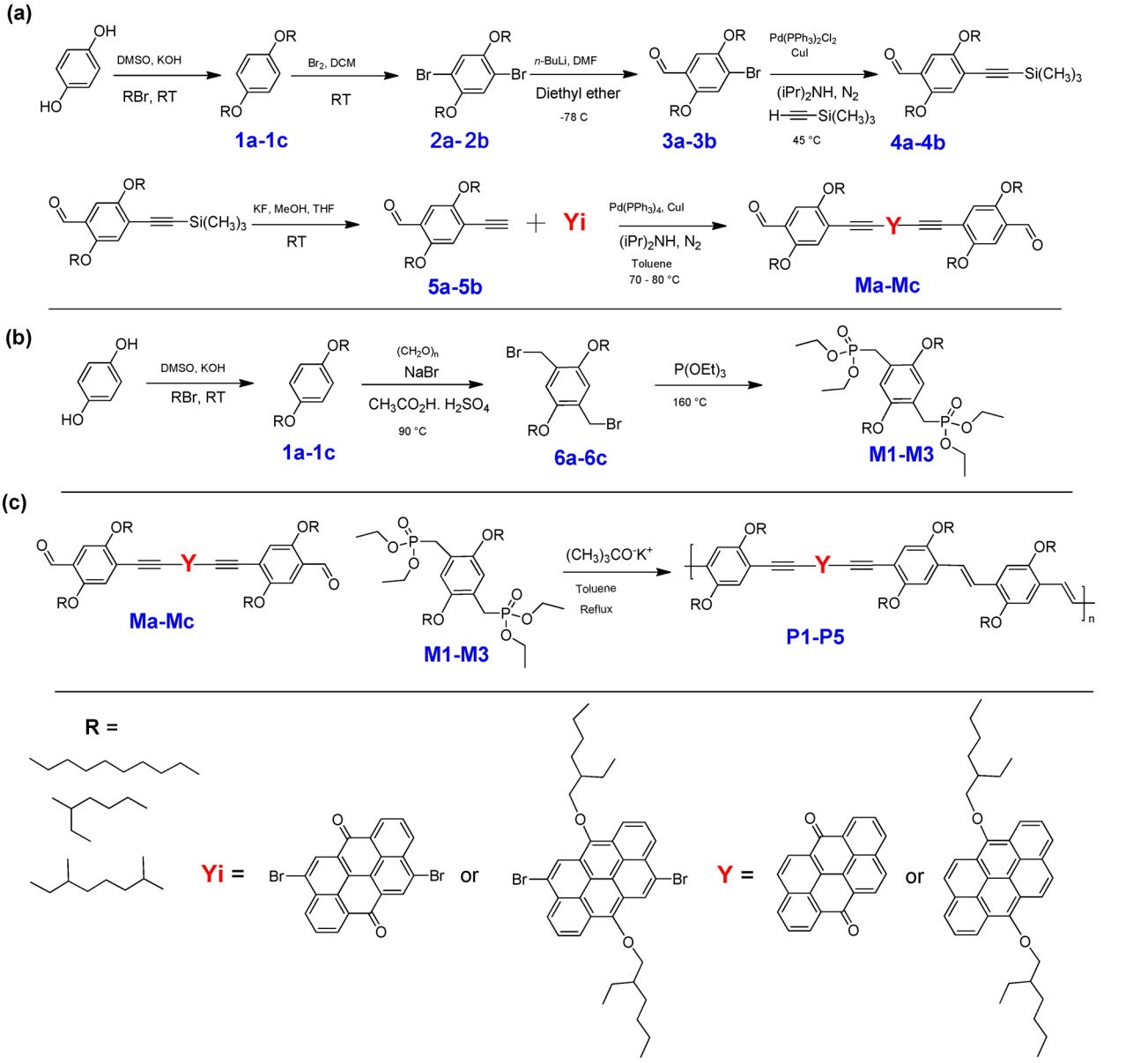

PAE-AVs are a class of polymeric materials that combine the intrinsic properties of poly(arylene ethynylene) (PAE) and poly(arylene vinylene) (PAV) into a single backbone with additional structure-specific properties.[31] The general constitutional unit of the PAE-AV backbones in this study, $(-Ph-C{\equiv}C-Anth-C{\equiv}C-Ph-CH{=}CH-Ph-CH{=}CH-)_n$, contains an anthanthrone or its analogue anthanthrene embedded between two alkyne moieties (Figure 1b). To the best of our knowledge, the use of anthanthrone and its derivative as building blocks for polymer synthesis via the PAE-AV backbone has never been reported. PAE-AV based on other structures such as anthracene,[32−41] thiophene and phenylene core[31,42,43] have been reported. The aim of the current study was to establish anthanthrone and its derivatives as suitable building blocks for the design of novel PAE-AV backbones with good solubility (through side chain incorporation and variation) and to study their suitability as emitting or absorber materials in organic light-emitting or photovoltaic (OPV) devices, respectively.

RESULTS AND DISCUSSION

Synthesis. The synthesis of new polymers is schematically displayed in Scheme 1. The synthesis of the dialdehydes **Ma−Mc** and the bisphosphonates **M1−M3** follows well-established protocols.[32,33,44,45] Starting both with the O-alkylation of hydroquinone, their preparation involves overall 6 and 3 reaction steps, respectively. The reaction sequence for the synthesis of the dialdehyde involves the dibromination of the O-alkylated hydroquinone; the transformation of one bromo substituent by formylation; the substitution of the remaining bromo substituent by trimethylsilylethynyl via palladium-catalyzed Sonogashira cross-coupling reaction; and the cleavage of the trimethylsilane group to yield an alkyne functionalization, which was reacted with the respective dibromo anthanthrone or anthanthrene derivative in the final Sonogashira cross coupling (Scheme 1a).

The chemical structure and purity of the synthesized materials were confirmed by NMR spectroscopy. The ^{1}H NMR, ^{13}C NMR and ^{31}P NMR spectra of the bisphosphonate

DOI: 10.1021/acs.macromol.7b02136
Macromolecules 2017, 50, 8357−8371

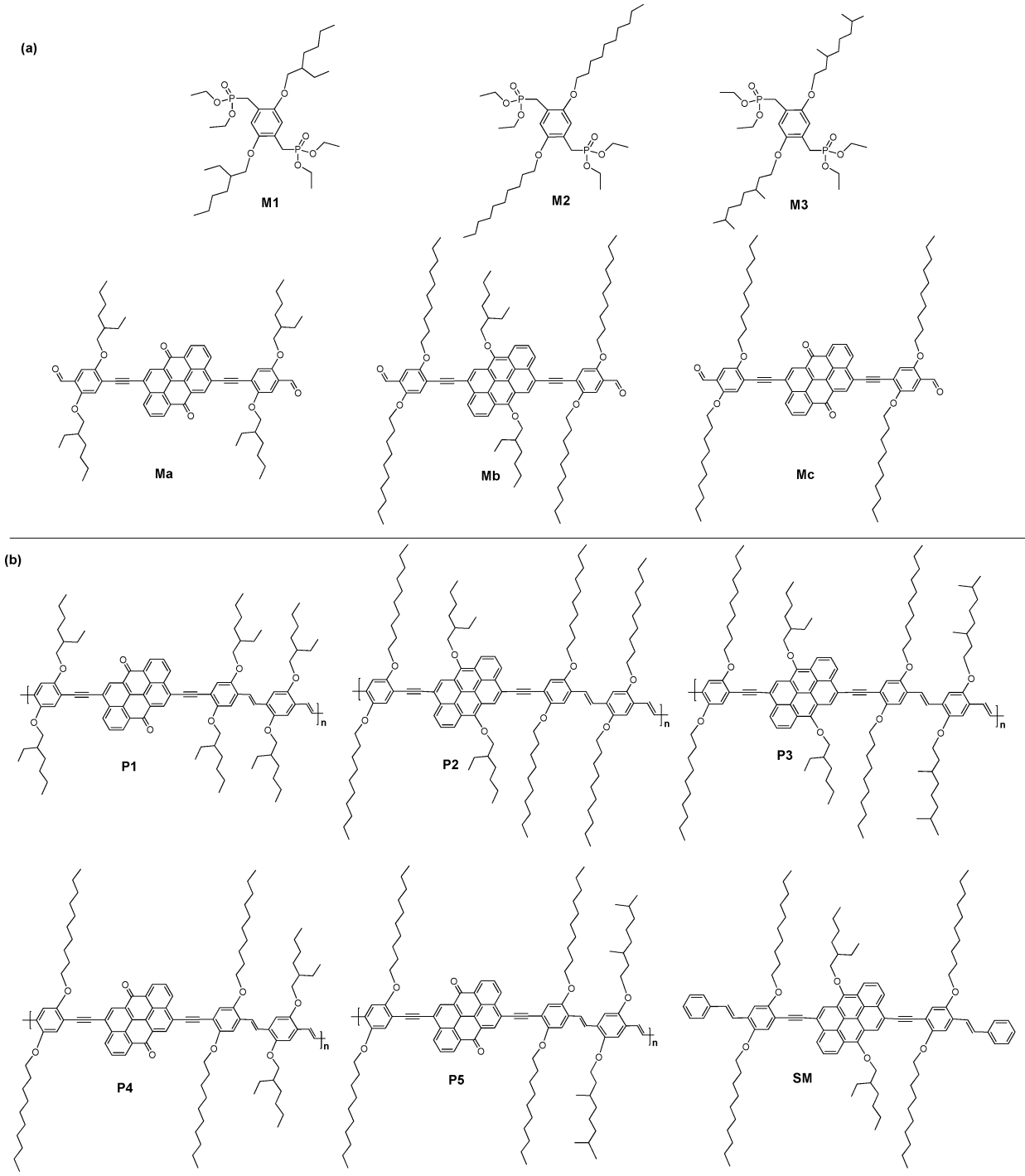

Figure 1. (a) Monomers (**M1**−**M3** and **Ma**−**Mc**) and (b) polymers (**P1**−**P5**) and a small molecule (**SM**).

polycondensation comonomers, **M1**, **M2**, and **M3**, are depicted in the Supporting Information (Figures S1−S9). The NMR spectra of the dialdehyde polycondensation comonomers, **Ma**−**Mc**, are displayed in Figures 2 and S10−S14. For the polymers **P1**, **P2**, and **P3**, ^{1}H NMR and FTIR spectroscopy were conducted (Figures 3 and S15−S20), while for **SM**, only ^{1}H NMR was conducted (Figure S21).

The NMR spectra of the bisphosphonate polycondensation comonomers (**M1**−**M3**, Figures S1−S9) are in good agreement with literature.[44−50] For **Ma**−**Mc**, the ^{1}H signals (Figure 2 and Figures S10−S12) in the range 10.49−10.44 ppm are attributed to the CHO aldehyde protons while the aromatic protons of the anthanthrone/anthanthrene unit and the phenylene group appear in the range 8.94−7.09 ppm. The CH_2 protons directly linked to the oxygen in the alkoxy side chain, in the phenyl group, as well as, in the anthanthrene unit, are visible in the 4.92−3.49 ppm region. The CH (ethylhexyloxy side chain) and CH_2 (decyloxy side chain) protons following the CH_2 groups directly linked to the oxygen of the alkoxy side chains are assigned to the signals in the range 2.36−1.68 ppm. All other CH_2 protons present in the compounds show signals in the range 1.68−1.03 ppm, while the signals of all CH_3 protons are clearly visible between 1.03 and 0.87 ppm. The ^{13}C spectra of

DOI: 10.1021/acs.macromol.7b02136
Macromolecules 2017, 50, 8357−8371

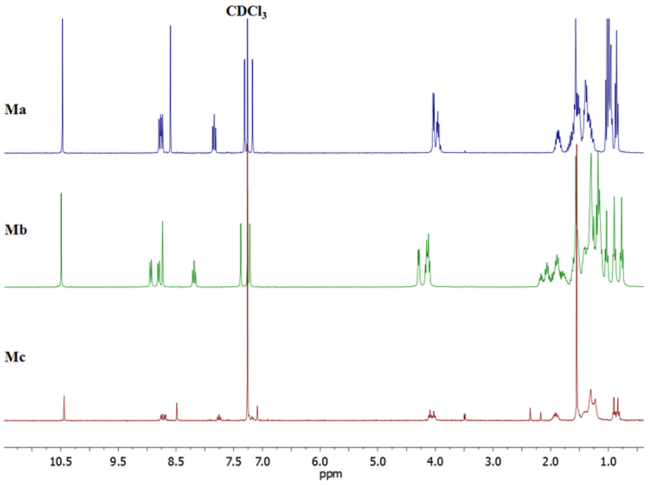

Figure 2. ^{1}H NMR spectra of **Ma**−**Mc**.

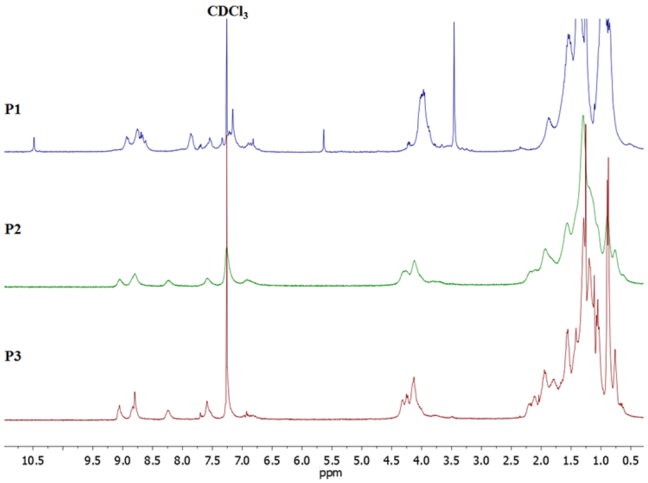

Figure 3. ^{1}H NMR spectra of **P1**−**P3**.

Ma and **Mb** have been schematically illustrated and explained as shown in Figures S13 and S14, respectively.

While the ^{1}H NMR spectra of the polycondensation comonomers, bisphosphonates, and dialdehydes are well-resolved and show defined signals, the spectra of the HWE polycondensation products are characterized by a distinct signal broadening and low resolution. The depletion or absence of the characteristic signals for the reactive functionalities of the comonomers, CHO (∼10.5 ppm) and CH_2−P (3.5 ppm), indicates the successful formation of polymeric species. The signals between 9.25 and 8.41 ppm in **P1** are assigned to the protons of the anthanthrone core. Between 8.07 and 6.67 ppm arylene vinylene proton signals can be identified. The signals in the region 4.37−3.20 ppm and 2.49−0.37 ppm are the protons of the alkyloxy side chains (Figure 3). The presence of a residual aldehyde signal in the ^{1}H NMR spectrum of **P1** (∼10.5 ppm) suggests that the soluble fraction of **P1** consists of low-molecular weight species with aldehyde end groups. Figure 3 shows the ^{1}H NMR signals of **P2** and **P3**. The broad NMR peaks occurring at 9.05−8.22 ppm are the anthanthrenylene protons and that at 7.65−6.92 ppm are due to the arylene vinylene protons. The peaks in the regions 4.61−3.28 ppm and 2.41−0.42 ppm are those of the protons of the alkoxy side chains. In contrast to **P1** the ^{1}H NMR spectra of **P2** and **P3** do not show any sign of a residual aldehyde signal.

Mc was applied in HWE polycondensation reactions with the bisphosphonate **M1** and **M3** to obtain the polymers **P4** and **P5**, respectively. However, the materials obtained from this reaction showed no reasonable solubility in common solvents, which prevented further characterization. Despite **P1**, **P4**, and **P5** possessing identical backbones based on anthanthrone units, the presence of only branched 2-ethylhexyloxy side chains apparently granted partial solubility for **P1** in common organic solvents. The linear decyloxy side chains in **P4** and **P5** appear much less efficient in promoting solubility. The significantly better solubility of the polymers **P2** and **P3** can be apparently attributed to the presence of anthanthrene instead of anthanthrone building blocks in the polymer backbones. The repeating units of **P2** and **P3** are isomeric. Their structures only differ in the side chains, linear dodecyloxy and branched (3,7-dimethyloctyl)oxy, introduced by the different bisphosphonates, which were used in the respective polycondensation reaction. This was done in order to study the effect of various side chains on the polymer properties.

The characteristic FTIR signals associated with the molecular vibrations of **P1**, **P2**, and **P3** occur at 3073−3064, 2962−2850, 2198−2180, 1659, 1603−1575, 1500, 1464, 1380, and 1203 cm^{-1} (Figures S18−S20). The bands between 3073−3064 cm^{-1} are attributed to the stretching vibrations of aromatic ═C−H and unsaturated hydrocarbon (vinylene). Characteristic aliphatic −C−H stretching vibrations of all three polymers show high intensity signals at 2962−2850 cm^{-1}, while the vibrational stretching of the ethynylene linker bond (−C≡C−) gives a weak signal at 2198−2180 cm^{-1} for all the three polymers. These FTIR spectral signals confirm a disubstituted ethynylene linker bond. The characteristic stretching vibration associated with the ketone group (−C═O) of **P1** is observed at 1659 cm^{-1}, and as expected, this ketone signal is completely absent in the spectra of **P2** and **P3**. The signals around 1603−1575 cm^{-1} are produced by the vinylene linker bond stretching, while those observed at 1500 and 1203−1031 cm^{-1} are for the stretching vibrations of aromatic −C═C− and aromatic−aliphatic −C═C−O−C− bonds, respectively. The bands observed at 969 and 861−869 cm^{-1} are attributed to the vinylene double bonds.

Molecular Mass and Thermal Studies. Results obtained from SEC (THF as eluent, polystyrene standards) and thermogravimetric analyses (TGA) are provided in Table 1.

Table 1. Synthesis and TGA Data of the Copolymers[a]

material	T (°C)	yield (%)	M_w[b] (g/mol)	$Đ$	T_d (°C)
P1	118	95	3570	2	325
P2	118	*95	11730	3.7	314
P3	118	*33	7820	2.7	331
P3	111	*73	11800	3.2	–

[a] T is the reaction temperature, M_w is the weight-average molecular weight, $Đ$ is the dispersity, and T_d is the thermal decomposition temperature @ 5% weight loss). [b] Measured by SEC in tetrahydrofuran as the mobile phase, and polystyrene standards were used for calibration. * Determined for the soluble fraction.

The molecular masses of the polymers **P1**, **P2**, and **P3** are relatively low. The difficulty in the preparation of polymers of high molecular masses that contain anthanthrone or anthanthrene building blocks, is apparent from the results obtained for polymers **P1**−**P3**. The low M_n value obtained for **P1** can be attributed to the rapid precipitation from the reaction mixture

DOI: 10.1021/acs.macromol.7b02136
Macromolecules 2017, 50, 8357−8371

during the polycondensation as a result of the poor solubility of the polymer. The thermogravimetric analysis (TGA) data indicates good thermal stability for all three polymers (**P1**, **P2**, and **P3**). Only a 5% weight loss was observed between 314 and 331 °C (Table 1 and Figure S22).

Photophysical Properties. The photophysical properties of the soluble polymers **P1**, **P2**, and **P3** and the anthanthrene small molecule (**SM**) (which is used as a model compound) were investigated by UV−vis absorption spectroscopy and photoluminescence spectroscopy, for both the solutions and thin films of the materials. The absorption spectra obtained for measurements taken with dilute solutions and thin films are displayed in Figures 4 and 5, respectively, and their characteristic data are summarized in Tables 2 and 3.

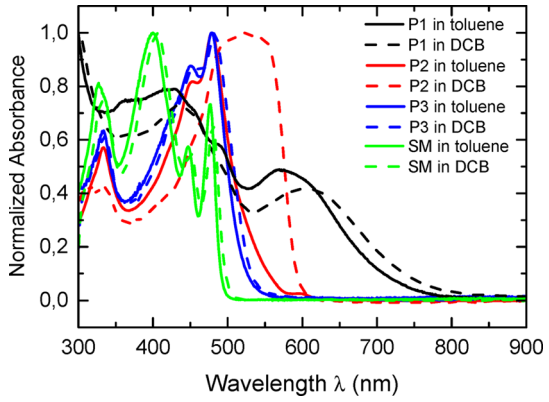

Figure 4. UV−vis absorption spectra of **P1** (black), **P2** (red), and **P3** (blue) copolymers, and **SM** (green) model compound measured in dilute toluene (solid curves) and DCB (dashed curves) solutions.

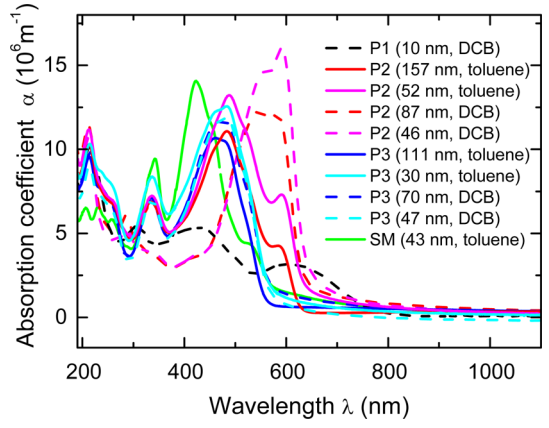

Figure 5. UV−vis absorption spectra of **P1** (black), **P2** (red for thicker and magenta for thinner films), **P3** (blue for thicker and cyan for thinner films), and **SM** (green) thin films prepared from toluene (solid) and DCB (dashed) solutions.

The absorption of **P1** covers the whole visible spectral region and its spectra exhibited broad absorption bands in both solutions and as thin films. The long wavelength maxima are located at 429 and 569 nm for measurements done in toluene and red-shifted to 433 and 607 nm in DCB solution spectra. In thin film spectra, the maxima were slightly blue-shifted (427, 604 nm) relative to the DCB solution spectra. The long-wavelength band can be assigned to the $\pi-\pi^*$ transition of the conjugated polymer backbone and the band at higher energy to the $n-\pi^*$ transition from the carbonyl of the anthanthrone moiety, which is also influenced by conjugation. It is noteworthy that only very thin films of good quality could be prepared by spin-coating due to the limited solubility of **P1**.

The absorption spectra of the **P2** and **P3** copolymers with anthanthrene unit significantly differ from the spectra of **P1**. The corresponding **SM** model compound for **P2** and **P3** exhibits well resolved absorption spectrum in toluene and DCB solutions that are typical of fused conjugated systems,[51−54] with maxima at 327, 400, 447, and 477 nm in toluene and slightly red-shifted maxima at 332, 405, 450, and 480 nm in DCB. The absorption spectrum of **SM** thin film is not so well resolved reflecting the intermolecular interactions in solid state. The absorption maxima of the thin film were red-shifted and an absorption extension of up to 550 nm was observed when compared with the spectra obtained for solution. The **P2** and **P3** exhibit broad-band absorption in solution and thin films. The absorption spectra in their toluene solutions are less resolved but similar for both **P2** and **P3** copolymers, with the main maximum occurring at 478 and 479 nm, respectively. **P2** exhibited more extended shoulder at long wavelengths. Qualitatively different absorption spectrum was observed for **P2** when measured in DCB solutions. The **P2** absorption spectrum in DCB solution (see Figure 4) shows broad structureless absorption in the visible region from 400 to 600 nm, which is red-shifted compared to its toluene solution spectrum and also the **P3** and **SM** spectra. Broad red-shifted band indicates more planar backbone configuration and also aggregate formation in DCB, whereas the **P3** DCB spectra are of similar shape to its absorption spectra measured in toluene with slightly red-shifted maxima. Similar absorption behavior as in **P2** toluene solution was observed in its tetrahydrafuran solution, and on the other hand, the aggregation was also observed in **P2** chloroform solution. The **P3** absorption spectrum is also red-shifted compared to the **SM** spectrum or its spectrum in toluene, but the red shift is not so pronounced. Two long-wavelength maxima at 455 and 483 nm can be well resolved in its DCB absorption spectra similarly to those of toluene solution. The broad band in **P2** absorption spectrum in DCB reflects more planar structure than **P3** and the molecular aggregation in dilute solution. In the case of **P2**, the absorption spectra of their thin films differ when the films are prepared from toluene or DCB solutions, whereas such difference was not observed for **P3** thin films. The absorption spectra of **P2** thin films prepared from DCB are significantly red-shifted and differ in shape from the absorption spectra of **P2** thin films prepared from toluene solution, which are blue-shifted.

New polymers **P2** and **P3** also exhibit PL emission in both solution and thin films, whereas the PL emission of new polymer **P1** was very weak, particularly in DCB solution and thin films. The **SM** model compound is a highly luminescent material in dilute solution. Therefore, PL properties of **P1** were studied in toluene solution and a more detailed PL study was performed for **SM**, **P2**, and **P3**. The PL excitation and emission spectra measured in toluene and DCB solutions are displayed in Figures 6 and 7, respectively, and the characteristic data are summarized in Table 2. In toluene solution (Figure 6), **P1** exhibits a PL main maximum at 612 nm when excited at long wavelength absorption maxima. If the excitation wavelength is shorter an additional maximum appeared at about 500 nm originating from anthranthrone-containing segments, which is supported by the different excitation spectra for the emission wavelengths for the 500 nm and the main maximum. In DCB solution the PL emission of **P1** is very weak. In toluene

DOI: 10.1021/acs.macromol.7b02136
Macromolecules 2017, 50, 8357−8371

Table 2. Photophysical Properties of the Copolymers Measured in Dilute Toluene and DCB Solutions (λ_{absmax}, Absorption Maximum; λ_{PLmax}, Emission Maximum; $\lambda_{PLexcmax}$, Maximum of the Excitation Spectrum; η_{PL}, Photoluminescence Quantum Yield; Primary Maxima in Bold)

material	solvent	λ_{absmax} (nm)	λ_{PLmax} [a] (nm)	$\lambda_{PLexcmax}$ [b] (nm)	η_{PL}
P1	toluene	363sh, 429, 487 sh, 569	502, **612**	**349**, 550	–
P1	DCB	433, 607	–	–	–
P2	toluene	333, 451, **478**	**519**, 554	332, 447, **478**	0.47[c]
P2	DCB	332, **492** (**523**)	533, **589**	337, 484, **530**	0.54[d]
P3	toluene	334, 450, **479**	**520**, 551	332, 450, **480**	0.47[c]
P3	DCB	334, 455, **483**	533	334, 451, **484**	0.53[c]
SM	toluene	327, **400**, 447, 477	**488**, 518	334, **396**, 447, 477	0.92[c]
SM	DCB	332, **405**, 450, 480	499	331, **405**, 449, 480	0.95[c]

[a]Excitation wavelength at λ_{absmax}; [b]Emission wavelength at λ_{PLmax}, [c]Fluorescein used as the standard. [d]Rhodamine 6G used as the standard.

Table 3. Photophysical Properties of the Copolymers Measured as Thin Films Prepared from Toluene or DCB (λ_{absmax}, Absorption Maximum; λ_{PLmax}, Emission Maximum; $\lambda_{PLexcmax}$, Maximum of the Excitation Spectrum; d, Film Thickness; Primary Maxima in Bold)

thin film	prepared from	d (nm)	λ_{absmax} (nm)	λ_{PLmax} [a] (nm)	$\lambda_{PLexcmax}$ [b] (nm)
P1	DCB	10	**213**, 304, 427, 604	–	–
P2	DCB	46	212, 286, 557, **591**	625	488, **531**, 571
P2	DCB	87	212, 286, **547**, 581	625	487, **529**, 570
P2	toluene	52	213, 336, **488**, 590	621	333, 457, **486**, 523, 577
P2	toluene	157	212, 336, **484**, 584	623	336, 458, **484**, 525, 589
P3	DCB	47	213, 337, **483**	609	335, **454**, 485
P3	DCB	70	213, 335, **479**	604	331, 451, **482**
P3	toluene	30	214, 337, **484**	605	335, **454**, 485
P3	toluene	111	213, 334, **462**	611	334, 456, **485**
SM	DCB	43	206, 231, 258, 342, **423**, 455 sh, 525 sh	567	339, **421**

[a]Excitation wavelength at λ_{absmax}; [b]Emission wavelength at λ_{PLmax}

solution, **P2** and **P3** emit yellowish light, which is red-shifted when compared with **SM** model compound's emission of greenish light. In DCB solution the **P2** emission is significantly red-shifted and the emitted light is of orange-red color whereas PL emission of **P3** is similar to its toluene solution. Similarly, as in the absorption study, the PL emission spectra of **P2** and **P3** measured in toluene solutions are similar, but significantly differ in DCB solutions. In the toluene solution, the emission spectra show vibration structure with main maxima at 519 and 520 nm for **P2** and **P3**, respectively, and the excitation ones are well resolved and follow absorption ones. In the DCB solution PL emission spectra of **P2** and **P3** (Figure 7, parts a and b) significantly differ. The PL maximum of **P2** DCB solution spectrum, located at 589 nm, significantly red-shifted when compared with the maximum of its emission spectrum in toluene and with the 533 nm of the **P3** DCB solution spectrum. The maximum at about 530 nm is also observed in the **P2** emission spectrum for the shorter excitation wavelength of 482 nm, but the maximum at 589 nm dominates.

The excitation spectra of **P2** in DCB depended on the emission wavelength. For the emission at 531 nm, the PL excitation spectrum is similar to that measured in toluene, whereas for the emission at 589 nm the PL excitation spectrum is broader with a better resolved structure, but it follows the shape of absorption spectrum in DCB. The excitation spectrum of **P3** exhibited better-resolved vibration structure when compared with the corresponding absorption spectra and follows well the shape of the absorption one. The PL behavior of **P2** supports the results from the absorption study concerning the better planarity and aggregation of **P2** molecules in the DCB. The PL quantum yields determined for **P2** and **P3** in their toluene and DCB solutions were similar for both polymers in the same solution, and both **P2** and **P3** have slightly higher values in their DCB solutions. PL emission and excitation spectra of the **SM** model compound are shown in Figures 6 and 7 for comparison. In toluene the PL emission spectrum for **SM** is better resolved and exhibited a maximum at 488 nm, whereas the maximum of the **SM** spectrum in DCB is slightly red-shifted at 499 nm. The excitation spectra are well resolved for both solvents and similar to the absorption ones.

The PL spectra measured for the thin films are displayed in Figure 8, and the characteristic data are summarized in Table 3. For the thin films, the emission maxima are red-shifted compared to their solutions. In the PL the emission maxima are at 621−623 nm in the spectra of **P2** films prepared from toluene and are slightly red-shifted to 625 nm for **P2** prepared from DCB. The shape of emission spectra is similar for both **P2** films, but the excitation spectra significantly differ. The excitation spectrum of **P2** film prepared from toluene follows a similar pattern to its absorption spectrum, but the excitation spectrum of the **P2** film prepared from DCB differs in shape from its absorption one. In the case of **P3** films the PL emission with maxima at 605−611 nm is slightly blue-shifted when compared with **P2** films and there is nearly no difference for the **P3** films prepared from toluene or DCB. The excitation spectra follow a similar behavior to those of the absorption ones and are better resolved. Compared with the toluene solution red shift in the emission maxima of the PL thin film spectra is about 100 nm for **P2** and 70 nm for **P3** films, which indicates excimer and/or aggregate formation in solid state for both polymers, which is also evident from the large Stokes shifts.

DOI: 10.1021/acs.macromol.7b02136
Macromolecules 2017, 50, 8357−8371

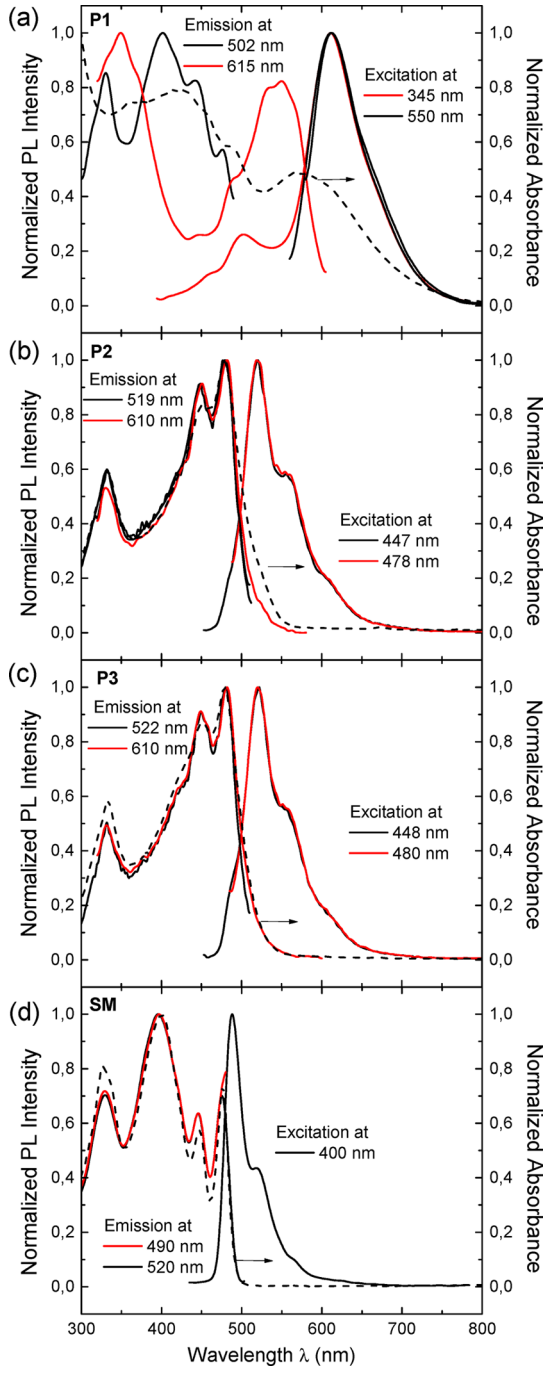

Figure 6. PL emission and excitation spectra of (a) **P1**, (b) **P2**, (c) **P3**, and (d) **SM** measured in dilute toluene solutions. Normalized absorption spectra are shown in dashed lines.

The PL spectra of **SM** thin film are also shown in Figure 8c. A red shift of the PL emission spectrum is also observed. The shape of the excitation spectrum matches well with the absorption spectrum shape. The relative PL efficiency of a thin film, Φ_{PLrel}, was used to compare the PL efficiencies of the polymers. The Φ_{PLrel} of the films prepared from toluene is similar for both copolymers **P2** and **P3**, whereas Φ_{PLrel} of **P2** films prepared from DCB is by more than three times higher than the Φ_{PLrel} of **P3**.

Electrochemical Properties. Cyclic voltammetry (CV) measurements were performed to obtain information on the electronic structures of the new polymers. Representative CV

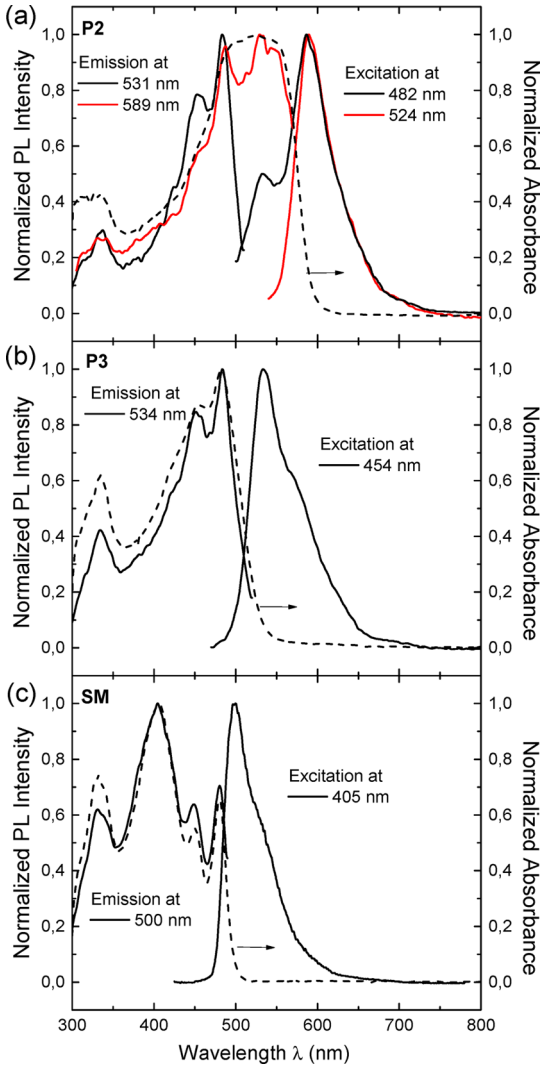

Figure 7. PL emission and excitation spectra of (a) **P2**, (b) **P3**, and (c) **SM** measured in dilute DCB solutions. Normalized absorption spectra are shown in dashed lines.

curves of **P1**, **P2**, and **P3** polymer thin films and **SM** film coated on a Pt wire are displayed in Figure 9. Quasi-reversibility in the oxidation and reduction of all new polymers and also **SM** model compound was observed. The ionization potential (HOMO level), E_{IP}, and electron affinity (LUMO level), E_A, were estimated from the onset potentials, E_{onset}, of the oxidation and reduction peaks based on the reference energy level of ferrocene (4.8 eV below the vacuum level) using the equation E_{IP} (E_A) = |−(E_{onset} − E_{ferr}) − 4.8| eV, where E_{ferr} is the half-wave potential for ferrocene vs the Ag/Ag^+ electrode. The CV curve of **SM** exhibited a small prepeak in the reduction, which is in good correlation with the shoulder in the thin film absorption spectra. The similar E_{IP} ($-E_{HOMO}$) values of 5.05, 5.12, and 5.15 eV were evaluated for **P2**, **P3** and **SM**, respectively, which are lower than the value of 5.36 eV obtained for **P1**. The E_A ($-E_{LUMO}$) value of 3.87 eV for **P1** was higher than 2.92, 2.85, and 2.62/2.84 eV evaluated for **P2**, **P3** and **SM**, respectively. The E_A values reflect the higher electron affinity of the anthanthrone block (which possesses two electron-withdrawing keto groups at the 6- and 12-positions of the anthanthrone unit) than the anthanthrene unit. Electrochemical bandgap values of 1.49, 2.13, and 2.27 eV were determined for

DOI: 10.1021/acs.macromol.7b02136
Macromolecules 2017, 50, 8357−8371

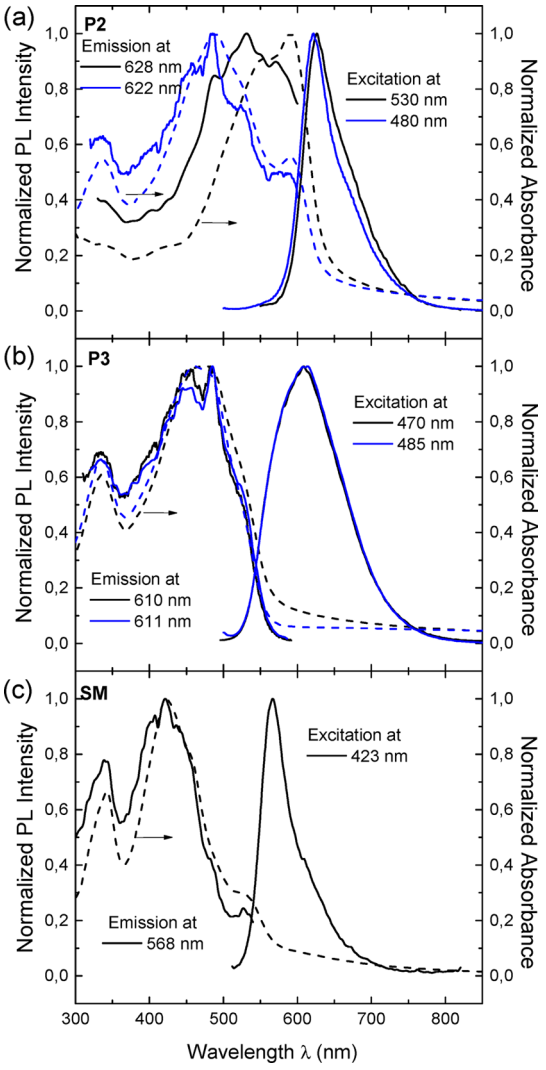

Figure 8. PL emission and excitation spectra of 52 nm (blue) and 46 nm (black) thick **P2** films, 111 nm (blue) and 70 nm (black) thick **P3** films prepared from toluene (blue) and DCB (black) solutions, respectively, and 43 nm thick **SM** prepared from DCB. Normalized absorption spectra are shown in dashed lines.

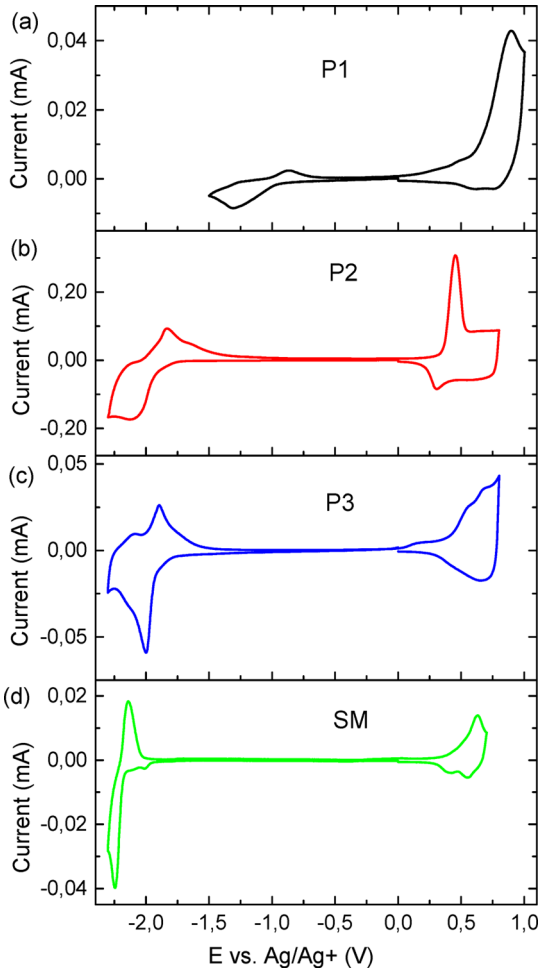

Figure 9. Representative cyclic voltammograms of (a) **P1**, (b) **P2**, (c) **P3**, and (d) **SM** thin films coated on a Pt wire, recorded at a scan rate of 50 mV s^{-1}.

P1, **P2** and **P3**, respectively, which were slightly higher values than the optical bandgap values determined from the absorption edge (except for **P1**), but there was good correlation between the values for the polymers and **SM**. (see Table 4).

Electroluminescent Properties. The new polymers **P2** and **P3** were used to create active layers in samples of light-emitting diodes (LEDs). LEDs with a hole-injecting electrode formed by indium-tin oxide (ITO) covered with a poly[3,4-(ethylenedioxy)thiophene]/poly(styrenesulfonate) (PEDOT:PSS) layer and an electron-injecting electrode of calcium covered with aluminum (Ca/Al) were prepared and studied. The electroluminescent (EL) spectra of the LEDs are shown in Figure 10. The EL spectrum of the **P2** LEDs was similar to the PL thin film spectrum. The EL emission maximum was at 624 nm. The EL spectra of **P3** LEDs were slightly blue-shifted to the PL thin film spectra. The EL maximum of the **P3** LEDs depended slightly on the applied voltage; a blue shift was observed as voltage increased. Similarity in EL and PL thin-film spectra indicated that similar centers occur in the EL and PL emission processes.

The **P2** LED exhibited better performance than the **P3** LED, which is in good agreement with the relative PL efficiencies of the thin films. An example of the typical dependences of the luminance on the applied voltage measured on the ITO/PEDOT:PSS/polymer/Ca/Al LED is shown in Figure 11. The **P2** LED produced higher luminance values (of up to 200 cd m^{-2}, where saturation occurred) and a lower EL onset voltage (of 1.9–2 V) than **P3**. Lower EL onset voltages for **P2** (in comparison with **P3**) are in good correspondence with the lower bandgap values of **P2** compared with **P3**. The EL results obtained with the nonoptimized simple LEDs gave an interesting comparison of the two new copolymers. **P2** seems to be more promising for further polymer or device optimization: for example, by the modification of the injection electrodes, or by using various blends of EL polymers (in the case of polymer-blend LEDs) with appropriate electroluminescent or charge-transporting polymers to make charge injection and transport more balanced.[55−62]

Photovoltaic Properties. To investigate the performance of the new polymers **P1**–**P3** as absorbers in bulk heterojunction solar cell applications, organic photovoltaic devices (OPVs) with nonoptimized configurations were fabricated and investigated. The OPV devices {ITO/PEI/Polymer:[60]-PCBM(1:2)/MoOx/Ag} consisted of active blend layers of **P1**, **P2**, and **P3** copolymers and the fullerene derivative [6,6]-

DOI: 10.1021/acs.macromol.7b02136
Macromolecules 2017, 50, 8357−8371

Table 4. Electronic Properties of the Copolymers (E_{IP}, Ionization Potential; E_A, Electron Affinity; E_g^{elc}, Electrochemical Bandgap; E_g^{opt}, Optical Bandgap)

material	E_{IP} (eV) ($-E_{HOMO}$)	E_A (eV) ($-E_{LUMO}$)	E_g^{elc} (eV)	E_g^{opt} (eV)
P1	5.36	3.87	1.49	1.6
P2	5.05	2.92	2.13	1.98
P3	5.12	2.85	2.27	2.21
SM	5.15	2.62/[a]2.84	2.53/[a]2.33	2.51/2.2

[a]Evaluated from the reduction prepeak onset.

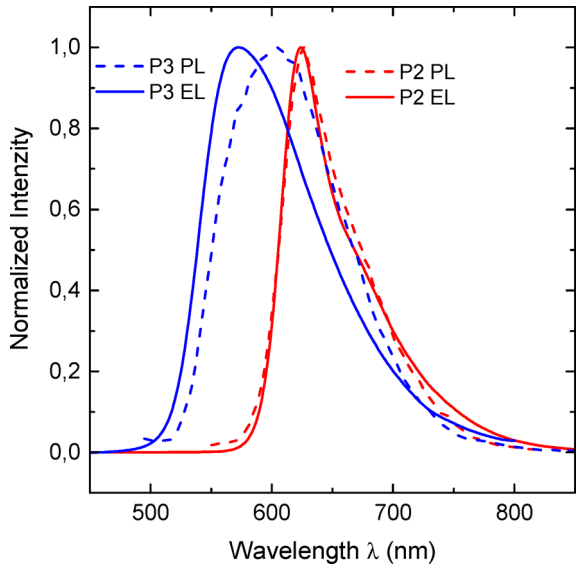

Figure 10. Normalized EL spectra (solid) of the ITO/PEDOT:PSS/**P2**/Ca/Al LED (blue) and ITO/PEDOT:PSS/**P3**/Ca/Al LED (red) measured at 3 V. PL emission spectra of the corresponding thin films (dashed) are displayed for comparison.

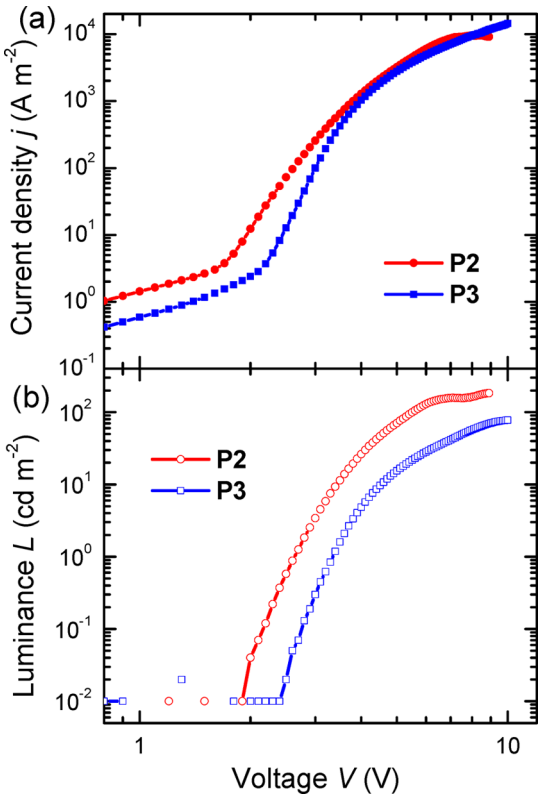

Figure 11. Dependence of current density (a) and luminance (b) on the applied voltage measured on the ITO/PEDOT:PSS/**P2**/Ca/Al (circles) and ITO/PEDOT:PSS/**P3**/Ca/Al (squares) LEDs.

phenyl-C61-butyric acid methyl ester ([60]PCBM), in an inverted cell architecture where polyethylenimine (PEI) and molybdenum oxide were used as interfacial layers. The current−voltage characteristics of the OPV devices involving **P1**−**P3** are shown in Figure 12, parts a and b. The OPVs based on **P2** and **P3** copolymers with anthranthrene unit exhibited better performance with power conversion efficiency (*PCE*) values of 1.17% and 0.61%, respectively, than the OPVs based on **P1** with anthranthrone unit having a *PCE* of 0.18% (Table 5).

The higher efficiency realized with **P2**-based OPV can be attributed to higher J_{sc} and *FF*. The V_{oc} ideally correlates with the energetic difference between the E_{IP} (HOMO) of the donor polymer and the E_A (LUMO) of the [60]PCBM acceptor. The OPVs based on **P2** and **P3** showed resemblance in their V_{oc} values (0.76 and 0.78 V, respectively), which is in good agreement with the similar ionization potentials E_{IP} (HOMO levels) of **P2** (5.05 eV) and **P3** (5.12 eV). The V_{oc} value for **P1** based OPV is higher (V_{oc} = 0.93 V) as expected due to higher E_{IP} value of **P1** (5.36 eV). The difference in the E_A values of the [60]PCBM and copolymer (LUMO energy offset) is for **P1** only 0.03 eV, which is probably too low value for exciton dissociation to be efficient enough, and this could implicate the low J_{SC} value for **P1** based OPV. On the other hand, LUMO energy offsets for **P2** and **P3** (of 1 eV) are large enough for the exciton dissociation. The E_A value of 3.9 eV used for [60]PCBM was obtained from our CV measurement. The low *FF* values of **P1** and **P3** based OPVs are likely to be attributed to nonsuitable film morphologies. The solubility of conducting polymers plays a major role in the film morphology. Low solubility leads to poor quality of films, which induce low *FF*s values and invariably lower the efficiency of OPV devices. Low solubility also seems to cause poor miscibility with the electron acceptor [60]PCBM, which might partly explain the limited performance of the devices. Besides other characteristics, generally the solubility, molecular weight, intermolecular interactions, and charge carrier mobilities of the conjugated semiconducting polymers can largely affect their photovoltaic properties.[63−68]

The external quantum efficiency (*EQE*), which is the measure of the efficiency of a cell to convert incident photons into free charge carriers, was also investigated. Figure 13 shows *EQE* curves for the OPVs. As a result, high *EQE* values can be achieved by the combined effect of efficient exciton generation in the bulk of the active blend layer, the dissociation into free charge carriers, and the charge transport to the respective electrode. The linear correlation between J_{sc} and *EQE* can be seen in **P1**−**P3** (Figure 13, Table 5). **P2** that has the highest J_{sc}

DOI: 10.1021/acs.macromol.7b02136
Macromolecules 2017, 50, 8357−8371

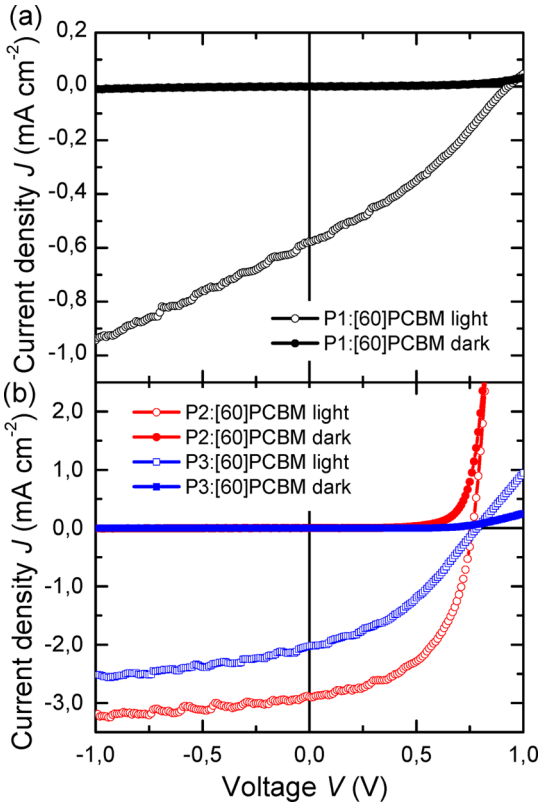

Figure 12. Current−voltage characteristics of ITO/PEI/polymer:[60]PCBM(1:2)/MoOx/Ag OPV devices using (a) **P1**, (b) **P2** (circles), and **P3** (squares), which were measured in the dark and under illumination by solar simulator at 100 mW cm^{-2}.

value exhibits the highest *EQE* value, while **P1**, with the lowest J_{sc}, has the lowest *EQE* value.

P1−**P3** were tested in OPV devices without any optimization and, therefore, the photovoltaic performance is also limited. Optimization of several parameters such as the morphology, variation of the mutual component ratio in blends and utilization of more appropriate device architecture could further improve the OPV devices.[63−68] We have recently shown that fullerene aggregation occurs in the blend layers, which can negatively influence the device performance.[69] Using blends with a nonfullerene acceptor for the active layer is another way to improve the stability and performance of OPV.[70−76]

CONCLUSIONS

Polycyclic aromatic building blocks based on anthanthrone and anthanthrene, were incorporated for the first time into the backbone of poly[(arylene ethynylene)-*alt*-(arylene vinylene)]s yielding new copolymers **P1**−**P5**. With copolymer **P1**, which possesses 4,10-linked anthanthrone building blocks and an all-branched 2-ethylhexyloxy side chains, it was possible to

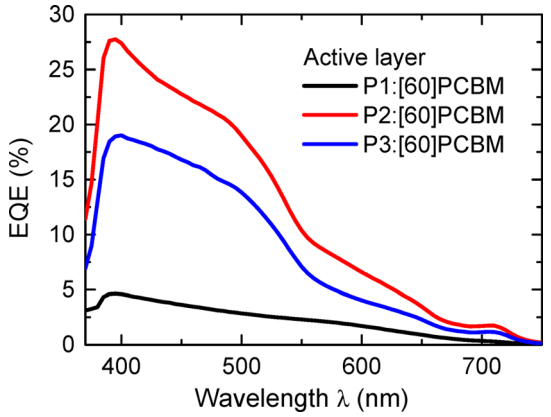

Figure 13. External quantum efficiencies of ITO/PEI/Polymer:[60]PCBM(1:2)/MoO_x/Ag OPV devices using **P1** (black), **P2** (red), and **P3** (blue).

demonstrate the preparation of the anthanthrone based PAE-AV polymer with soluble fractions. This was not possible with **P4** and **P5** with linear decyloxy side chains formed as insoluble materials. Substitution of anthanthrone with anthanthrene units appeared to be an efficient strategy to prepare polymers with appreciable solubility (**P2** and **P3**). **P1**, **P2**, and **P3** were studied in detail. All three polymers exhibited interesting photophysical properties. The absorption spectrum of **P1** in solution and thin films covered the whole visible spectral region. The PL of **P1** was weak, particularly in DCB and thin films. The "transformation" of the anthanthrone's carbonyl groups into anthanthrene's alkyloxy substituents in the synthesis of **P2** and **P3** affected the photophysical properties of the resultant copolymers significantly. The properties of **P2** and **P3** indicated that they were not only dominated by the polycyclic chromophore, but were also influenced by the nature of the side chains on the phenylene−vinylene unit (decyloxy in **P2** and 3,7-dimethyloctyloxy in **P3**). The absorption and PL properties of **P2** and **P3** were similar in their toluene solution only, whereas in DCB solutions they differ. The absorption spectra of **P2** thin films differed whether the thin films were prepared from toluene or from DCB solutions, contrary to **P3** thin films for which such a difference was not observed. PL studies also revealed differences in the **P2** and **P3** behavior in solutions and thin films. The results of the photophysical studies indicate the formation of aggregates in **P2** DCB solution, and more pronounced planarity and excimer or aggregate formation in **P2** films than in **P3** ones. The ionization potential (HOMO level) and electron affinity (LUMO level) values determined for **P1** were higher than the corresponding values for **P2** and **P3**, thereby reflecting the higher electron affinity of anthanthrone block than that of anthanthrene unit. The copolymers **P2** and **P3** were tested as active layers in polymer LEDs. The performance of the LEDs with **P2** as an active layer was better than that of the **P3** LEDs, which is in

Table 5. Photovoltaic Characteristic Data of ITO/PEI/Polymer:[60]PCBM(1:2)/MoOx/Ag Devices Based on P1, P2, and P3 (J_{sc}: short-circuit current density; V_{oc}: open-circuit voltage; *FF*: fill factor; *PCE*: power conversion efficiency; *d*: active layer thickness)

polymer	*d* (nm)	J_{sc} (mA cm^{-2})	V_{oc} (V)	*FF*	*PCE* (%)	*J* @ −2 V (mA cm^{-2})	*J* @ + 2 V (mA cm^{-2})
P1	92	0.58	0.93	0.33	0.18	−0.94	0.05
P2	104	2.90	0.76	0.53	1.17	−3.19	22.74
P3	134	2.02	0.78	0.39	0.61	−2.53	0.95

DOI: 10.1021/acs.macromol.7b02136
Macromolecules 2017, 50, 8357−8371

good agreement with the relative PL efficiencies of the thin films. **P1**, **P2**, and **P3** containing [60]PCBM in blend layers were also tested for photovoltaic applications. Similarly, photovoltaic devices based on **P2** exhibited better performance than those based on **P3**. The replacement of decyloxy side chains in **P2** with 3,7-dimethyloctyloxy in **P3** resulted in lower yield and decrease in photovoltaic efficiency. Optimization of the device composition and architecture might yield significant enhancements of the LED efficiency and the photovoltaic performance.

EXPERIMENTAL SECTION

Synthesis. All starting materials and solvents were purchased from commercial suppliers (Sigma-Aldrich, Merck and Alfa Aesar and VWR). Most of the details describing the synthesis steps toward the HWE polycondensation monomers, dialdehydes (**Ma**−**Mc**) and bisphosphonates (**M1**−**M3**) (Scheme 1), are given in the Supporting Information.

*Monomer Synthesis. Synthesis of **M1**.* A mixture of 1,4-bis(bromomethyl)-2,5-bis(2-ethylhexyloxy)benzene (15.2 g, 18.97 mmol) and an excess of triethylphosphite (9.47 g, 57.0 mmol) was stirred and heated slowly to 150−160 °C; simultaneously, the evolving ethyl bromide was distilled off. After 4 h, vacuum was applied for 30 min at 180 °C to distill off the excess triethylphosphite. The residual oily product was allowed to cool to room temperature (14.4 g, 83% yield). ^{1}H NMR (300 MHz, $CDCl_3$): δ 6.92 (d, J = 1.6 Hz, 2H), 4.08−3.89 (m, 8H), 3.79 (d, J = 5.6 Hz, 4H), 3.15 (d, J = 20.1 Hz, 4H), 1.76−1.59 (m, 2H), 1.55−1.34 (m, 10H), 1.34−1.11 (m, 18H), 0.99−0.63 (m, 12H). ^{13}C NMR (75 MHz, $CDCl_3$): δ 150.43, 119.30, 114.50, 71.17, 61.8, 39.65, 30.58, 29.09, 27.06, 25.21, 23.89, 23.00, 16.30, 14.01, 11.12.

M2 and **M3** were prepared under similar reaction conditions as described for **M1**

*Synthesis of **M2**.* A mixture of 1,4-bis(bromomethyl)-2,5-bis-(decyloxy)benzene (3.37 g, 5.85 mmol) and an excess of triethylphosphite (3.0 g, 17.6 mmol) were stirred and heated slowly to 150−160 °C, and the evolving ethyl bromide was distilled off simultaneously. The reaction proceeded for 4 h, after which vacuum was applied for 1 h at 180 °C to distill off any excess of triethylphosphite left in the mixture. The resulting oil was allowed to cool to room temperature to form a white solid, which was recrystallized from diethyl ether (30 mL), yielding a white powder (3.9 g, 97%). ^{1}H NMR (400 MHz, $CDCl_3$): δ 6.89 (s, 2H), 4.00 (m, 8H), 3.90 (t, J = 6.5 Hz, 4H), 3.20 (d, J = 20.3 Hz, 4H), 1.82−1.65 (m, 4H), 1.41−1.15 (m, 40H), 0.86 (t, J = 6.6 Hz, 6H). ^{13}C NMR (100 MHz, $CDCl_3$): δ 150.31, 119.28, 114.70, 68.89, 61.69, 31.89, 29.61, 29.56, 29.47, 29.44, 29.32, 26.92, 26.13, 25.54, 22.67, 16.38, 16.34, 16.31, 14.10.

*Synthesis of **M3**.* A mixture of 1,4-bis(bromomethyl)-2,5-bis(3,7-dimethyloctyloxy)benzene (5.10 g, 8.70 mmol) and an excess of triethylphosphite (4.40 g, 26.1 mmol) was stirred and heated slowly to 150−160 °C, and the evolving ethyl bromide was concurrently distilled off. After 4 h, vacuum was applied for 30 min at 180 °C to distill off any excess of triethylphosphite. The residual yellow oil was allowed to cool to room temperature (5.73 g, 96% yield). ^{1}H NMR (400 MHz, $CDCl_3$): δ 6.85 (s, 2H), 4.07−3.79 (m, 12H), 3.14 (d, J = 20.4 Hz, 4H), 1.86−1.37 (m, 8H), 1.32−1.01 (m, 24H), 0.86 (d, J = Hz, 6H), 0.79 (d, J = 6.6 Hz, 12H). ^{13}C NMR (100 MHz, $CDCl_3$): δ 150.15, 119.18, 114.60, 67.01, 61.61, 38.99, 37.09, 36.23, 29.63, 27.72, 26.71, 25.32, 24.45, 22.45, 22.34, 19.44, 16.09.

*Synthesis of **Ma**.* 4,10-Dibromoanthanthrone (408 mg, 0.88 mmol) was given to a mixture of diisopropylamine (15 mL) and tetrahydrofuran (40 mL). After deaeration of the reaction for 30 min, $Pd(PPh_3)_4$ (45.1 mg, 0.04 mmol) and CuI (7.4 mg, 0.04 mmol) were added. The mixture was allowed to stir and deaerate for another 30 min. Thereafter, 2,5-bis(2-ethylhexyloxy)-4-ethynylbenzaldehyde (750 mg, 2.0 mmol, dissolved in deaerated THF) was added dropwise. The reaction mixture was heated to 60 °C for 72 h in a nitrogen atmosphere. Thin layer chromatography (TLC) was used to monitor the progress of the reaction. Toluene (40 mL) was added and the heating was removed. After cooling to room temperature, the mixture was precipitated in cold methanol and refrigerated for 4 h. The precipitate was filtered off, redissolved in toluene, and purified through column chromatography (silica gel) toluene as eluent to yield 350 mg (37%) of a purplish black substance. ^{1}H NMR (300 MHz, $CDCl_3$): δ 10.47 (s, 2H), 8.87−8.66 (m, 4H), 8.60 (s, 2H), 7.95−7.73 (m, 2H), 7.32 (s, 2H), 7,17 (s, 2H), 4.17−3.82 (m, 8H), 2.03−1.73 (m, 4H), 1.73−1.16 (m, 32H), 1.1−0.8 (m, 24H). ^{13}C NMR (100 MHz, $CDCl_3$): δ 188.98, 182.12, 155.49, 154.07, 134.07, 133.74, 131.28, 129.53, 129.30, 128.63, 127.60, 125.45, 124.11, 119.09, 117.49, 109.36, 94.20, 93.96, 71.72, 71.65, 39.57, 39.48, 30.65, 30.34, 29.71, 29.14, 29.01, 24.04, 23.77, 23.11, 23.08, 14.13, 14.07, 11.26, 11.06.

*Synthesis of **Mb**.* A mixture of 4,10-dibromo-6,12-bis(2-ethylhexyloxy)anthanthrene (200 mg, 0.29 mmol), diisopropylamine (10 mL), and toluene (20 mL) was deaerated for 30 min. $Pd(PPh_3)_4$ (16.7 mg, 0.015 mmol), and CuI (2.8 mg, 0.02 mmol) were added. After another hour a deaerated solution of 2,5-bis(decyloxy)-4-ethynylbenzaldehyde (320 mg, 0.72 mmol) in toluene (15 mL) was added dropwise into the mixture. The reaction mixture was heated to 70−80 °C for 24 h in a nitrogen atmosphere and monitored with TLC. Toluene (40 mL) was added. After the reaction cooled to room temperature, the precipitated diisopropylammonium bromide was filtered off and the solvent was evaporated under vacuum. The residue was subjected to column chromatography−silica gel with toluene:hexane (4:1) as eluent. 380 mg (93% yield) of a greenish substance was obtained. ^{1}H NMR (300 MHz, $CDCl_3$): δ 10.49 (s, 2H), 8.94 (d, J = 7.4 Hz, 2H), 8.80 (d, J = 8.1 Hz, 2H), 8.73 (s, 2H), 8.19 (m, 2H), 7.38 (s, 2H), 7.22 (s, 2H), 4.29 (d, J = 5.5 Hz, 4H), 4.21−4.07 (m, 8H), 2.23−1.68 (m, 10H), 1.68−1.08 (m, 78H), 1.03 (t, J = 7.0 Hz, 6H), 0.90 (t, J = 6.6 Hz, 6H), 0.77 (t, J = 6.7 Hz, 6H). ^{13}C NMR (100 MHz, $CDCl_3$): δ 189.13, 155.51, 153.95, 150.13, 130.72, 127.58, 125.98, 125.61, 124.88, 124.52, 123.95, 121.27, 120.54, 120.22, 119.50, 117.12, 109.28, 96.16, 90.48, 69.26, 59.55, 41.30, 38.17, 31.94, 31.86, 31.26, 30.48, 29.70, 29.62, 29.46, 29.32, 26.12, 24.03, 23.31, 22.72, 22.58, 14.32, 14.15, 14.05, 11.56.

*Synthesis of **Mc**.* A mixture of 4,10-dibromoanthanthrone (200 mg, 0.43 mmol), diisopropylamine (12 mL), and toluene (20 mL) was deaerated. $Pd(PPh_3)_4$ (20.3 mg, 0.02 mmol) and CuI (3.3 mg, 0.02 mmol) were added. After 30 min, a deaerated solution of 2,5-bis(decyloxy)-4-ethynylbenzaldehyde (390 mg, 0.88 mmol) in toluene was added dropwise. The reaction mixture was heated to 70−80 °C for 24 h in a nitrogen atmosphere. Toluene was added and the mixture was allowed to cool to room temperature. The precipitated diisopropylammonium bromide was filtered off and the solvent was distilled off using a rotary evaporator. The residue was subjected to column chromatography using silica gel, with toluene as eluent to yield 130 mg (26% yield) of a purple substance. The same reaction was conducted in THF at 60 °C for 72 h. After cooling, the mixture was reprecipitated in cold methanol (100 mL). The precipitate was recovered via filtration, and the crude residue was purified by column chromatography (silica gel) with toluene as eluent to afford **Mc** as a purplish black solid (74% yield). ^{1}H NMR (300 MHz, $CDCl_3$): δ 10.44 (s, 2H), 8.72 (d, d, J = 6.9 Hz, 4H), 8.49 (s, 2H), 7.82−7.68 (m, 2H), 7.24−7.13 (m, 2H), 7.09 (s, 2H), 4.06 (t, t, J = 6.6 Hz, 8H), 2.17 (m, 4H), 1.91 (m, 8H), 1.66−1.08 (m, 56H), 0.87 (t, t, J = 6.2 Hz, 6H, 6H). Acquisition of the ^{13}C NMR spectrum of **Mc** proved unsuccessful because of the poor solubility and precipitation of the product during the course of the acquisition.

*Polymer Synthesis. Synthesis of **P1**.* For the synthesis of **P1**, a solution of **Ma** (150 mg, 0.14 mmol) and **M1** (89.0 mg, 0.14 mmol) in dry toluene (12 mL) was mechanically stirred and heated under nitrogen to reflux. The polymerization was initiated by the addition of potassium *tert*-butoxide (63.0 mg, 0.56 mmol) and a spontaneous color change from deep pink to black was observed. The reaction mixture was stirred for 45 min, and toluene (100 mL) was added. The reaction was quenched with aqueous HCl (10 wt %, 10 mL). The organic phase was separated and washed with deionized water until a pH of ∼7 was obtained. Residual water was removed from the mixture

DOI: 10.1021/acs.macromol.7b02136
Macromolecules 2017, 50, 8357−8371

by heating to reflux in a Dean−Stark apparatus. The water-free mixture was concentrated with a rotary evaporator, precipitated in cold methanol, and then kept in the refrigerator for 24 h. Afterward the precipitate was filtered off in a Soxhlet thimble, which was transferred into a Soxhlet extractor. Extraction was performed with methanol in order to remove oligomers and any impurity. The extraction continued until the extract appeared colorless. The polymer was redissolved in toluene, reprecipitated in cold methanol and stored in the refrigerator. After 24 h, it was filtered and dried under air to obtain a black, partially soluble polymeric material (190 mg, 95% yield). SEC of the soluble fractions (THF as eluent; polystyrene standards): M_n = 1830 g/mol, M_w = 3570 g/mol, and $Đ$ = 2. ^{1}H NMR of the soluble fractions (300 MHz, $CDCl_3$): δ 10.48 (s), 9.25−8.41 (m, anthanthronylene H's), 8.07−6.67 (m, arylene vinylene H's), 4.37−3.20 (m, $-CH_2O-$), 2.49−0.37 (m, alkyl H's). FTIR, cm^{-1}: 3064 (ν(=C−H)), 2962, 2934, and 2878 (ν(C−H)), 2198 (ν(C≡C)), 1659 (ν(C=O)), 1575 (ν(C=C) vinylene), 1500 (ν(C=C) aromatic ring), 1464 (δ(CH_2)), 1380 (δ(CH_3)), 1203 (ν(C=C−O−C) aromatic−aliphatic).

P2−P5 were prepared under similar reaction conditions as described for **P1**

Synthesis of P2. A solution of **Mb** (170 mg, 0.12 mmol) and **M2** (83.0 mg, 0.12 mmol) in dry toluene (12 mL) was mechanically stirred and heated under nitrogen to reflux. Potassium *tert*-butoxide (54 mg, 0.48 mmol) was added at a stable temperature to initiate the reaction. A color change from bright green to dark green was observed. The reaction mixture was stirred for 80 min. Thereafter, toluene (100 mL) was added, and the reaction was quenched with aqueous HCl (10 wt %, 10 mL). The mixture was cooled to room temperature; the organic phase separated and washed with deionized water until a pH of ∼7 was obtained. Residual water was removed from the mixture by heating to reflux in a Dean−Stark apparatus. The obtained solution was concentrated, precipitated in cold methanol, and kept in the refrigerator for 24 h. Afterward the precipitate was filtered off, transferred into a Soxhlet extractor, and extracted using methanol. The polymer was redissolved in chloroform and reprecipitated in cold methanol. It was filtered and dried for 24 h to obtain a brownish green polymeric material (220 mg, 95% yield). SEC (THF as eluent; polystyrene standards): M_n = 3200 g/mol, M_w = 11 730 g/mol, and $Đ$ = 3.7. ^{1}H NMR (300 MHz, $CDCl_3$): δ 9.05−8.22 (anthanthrenylene H's), 7.58−6.92 (arylene vinylene H's), 4.28−3.28 (m, $-CH_2O-$), 2.41−0.42 (m, alkyl H's). FTIR, cm^{-1}: 3064 (ν(=C−H)), 2962, 2924, and 2850 (ν(C−H)), 2180 (ν(C≡C)), 1594 (ν(C=C) vinylene), 1500 (ν(C=C) aromatic ring), 1464 (δ(CH_2)), 1203 (ν(C=C−O−C) aromatic−aliphatic).

Synthesis of P3. **P3** was obtained from a solution of **Mb** (190 mg, 0.14 mmol) and **M3** (93 mg, 0.15 mmol) in dry toluene (13 mL). The polymerization was initiated by the addition of potassium *tert*-butoxide (60 mg, 0.56 mmol). A color change from bright green to dark green was observed. The reaction mixture was stirred for 80 min. Chloroform (100 mL) was thereafter added, and the reaction was quenched with aqueous HCl (10 wt %, 10 mL). Mixture was cooled to room temperature; the organic phase was separated and washed with deionized water until a pH of ∼7 was obtained. Residual water was removed from the mixture by heating to reflux in a Dean−Stark apparatus. The obtained solution was concentrated, precipitated in cold methanol, and kept in the fridge for 24 h. Afterward the precipitate was filtered off using a thimble, transferred into a Soxhlet extractor, and extracted with methanol. The polymer was redissolved in chloroform and reprecipitated in methanol. It was filtered and dried to obtain a brownish green polymeric material. This polymerization was conducted twice using different oil bath temperatures, 111 °C [SEC (THF as eluent; polystyrene standards): M_n = 3650 g/mol, M_w = 11 800 g/mol, $Đ$ = 3.2] and 118 °C [SEC (THF as eluent; polystyrene standards): M_n 2880 g/mol, M_w 7820 g/mol, and $Đ$ = 2.7]. The polycondensation reaction conducted at 111 °C yielded material that is soluble in common organic solvents (180 mg, 73% yield). The reaction performed at higher temperature(118 °C) yielded material only partially soluble at elevated temperatures (33% yield). ^{1}H NMR (300 MHz, $CDCl_3$): δ 8.73 (m, (anthanthreneylene H's)), 7.65−6.90 (m, arylene vinylene H's), 4.61−3.48 (m, $-CH_2O-$), 2.38−0.42 (m, alkyl H's). FTIR, cm^{-1}: 3073 (ν(=C−H)), 2962, 2924, and 2850 (ν(C−H)), 2198 (ν(C≡C)), 1603 (ν(C=C) vinylene), 1500 (ν(C=C) aromatic ring), 1464 (δ(CH_2)), 1203 (ν(C=C−O−C) aromatic−aliphatic).

P4 and **P5** were synthesized under similar reaction conditions as described for **P1−P3**. For **P4**, monomers **Mc** and **M1** were employed while for **P5**; monomers **Mc** and **M3** were employed. Both polycondensation reactions produced materials that appeared completely insoluble and could not be further characterized.

Synthesis of SM. **Mb** (190 mg, 0.14 mmol) and diethyl benzylphosphonate (79.0 mg, 0.34 mmol) were dissolved in dried toluene (15 mL) to give a greenish brown color while stirring vigorously under nitrogen and heating under reflux. Potassium-*tert*-butoxide (62 mg, 0.50 mmol) was added (and the reaction mixture was heated at reflux for 30 min. After 30 min, toluene was added, heat was removed, and aqueous HCl (10 wt %) was added. The purification process yielded a greenish material (170 mg, 79%). ^{1}H NMR (300 MHz, $CDCl_3$): δ 9.08 (d, J = 7.3 Hz, 2H), 8.92−8.78 (m, 2H), 8.27 (t, J = 7.7 Hz, 2H), 7.64 (d, J = 7.6 Hz, 4H), 7.56−7.18 (m, 16H), 4.37 (d, J = 5.2 Hz, 4H), 4.28 (t, J = 6.4 Hz, 4H), 4.15 (t, J = 6.2 Hz, 4H), 2.19 (m, 2H), 1.94−1.03 (m, 80H), 0.94 (d, J = 6.6 Hz, 12H), 0.83 (t, J = 6.2 Hz, 12H).

Instrumentation. NMR spectra were recorded in $CDCl_3$ with a Gemini 300 MHz spectrometer and a Bruker Avance IIIHD 400 MHz Nanobay NMR spectrometer equipped with a 5 mm BBO. Fourier transform infrared (FTIR) spectroscopy was performed with a PerkinElmer ATR TWO FTIR Spectrometer at room temperature. Size exclusion chromatography (SEC) measurements were performed using a Pump Deltachrom (Watrex Comp.) with a Midas autosampler and two columns of MIXED-B LS PL gel, particle size 10 μm. An evaporative light scattering detector (PL-ELS-1000 from Polymer Laboratories) was used; THF was the mobile phase and polystyrene standards were used for calibration. Thermogravimetric analysis (TGA) were performed using PerkinElmer TGA 7 in the range between 20 and 600 °C at a heating rate of 10 K/min in nitrogen atmosphere.

Sample Preparation. Thin films were prepared by spin-coating from toluene and 1,2-dichlorobenzene solutions. Thin films were spin-coated onto fused silica substrates for optical studies or coated on a Pt wire electrode by dipping for electrochemical measurements. For polymer light-emitting devices (LED), polymer layers were prepared on indium−tin oxide (ITO) substrates covered with a thin layer of poly[3,4-(ethylenedioxy)thiophene]/poly(styrenesulfonate) (PEDOT:PSS). All polymer films were dried in a vacuum (10^{-3} Pa) at 353 K for 2 h. The ITO glass substrates were purchased from Merck (Germany). PEDOT:PSS (CLEVIOS P VP AI 4083) from Heraeus Clevios GmbH (Germany) was used for LED preparation. The 50 nm thick PEDOT:PSS layers were prepared by spin-coating and dried in air at 396 K for 15 min. The calcium (20 nm) and, subsequently, 60−80 nm thick aluminum electrodes were vacuum-evaporated on top of the polymer films to form LEDs. Typical active areas of the LEDs were 4 mm^2. Layer thicknesses were measured using a KLA-Tencor P-10 profilometer. All thin film preparations and the device fabrication were carried out in a glovebox under a nitrogen atmosphere. For the fabrication of organic photovoltaic (OPV) devices ITO-coated glass substrates (15 Ω/sq, Xin Yan Tech. LTD) were employed. Polymer blend layers composed of polymer and [60]PCBM (Sigma-Aldrich) were spin-coated on the ITO substrate covered with polyethylenimine (PEI). PEI was treated at 378 K. The MoO_x (10 nm) and, subsequently, 100 nm thick silver (Ag) electrodes were vacuum-evaporated on top of the polymer films to finalize OPVs. The thickness of the films was characterized with a Bruker DektakXT profilometer.

Cyclic Voltammetric Measurements. Cyclic voltammetry (CV) was performed with a PA4 polarographic analyzer (Laboratory Instruments, Prague, CZ) with a three-electrode cell. Platinum (Pt) wire electrodes were used as both working and counter electrodes. A nonaqueous Ag/Ag$^+$ electrode (Ag in 0.1 M $AgNO_3$ solution) was used as the reference electrode. CV measurements were made in an electrolyte solution of 0.1 M tetrabutylammonium hexafluorophos-

DOI: 10.1021/acs.macromol.7b02136
Macromolecules 2017, 50, 8357−8371

phate ($(TBA)PF_6$) in anhydrous acetonitrile under a nitrogen atmosphere in a glovebox. Typical scan rates were 20, 50, and 100 mV s^{-1}.

Photophysical Measurements. UV−vis spectra were measured on a PerkinElmer Lambda 35 UV/vis spectrometer. Solvents of spectroscopic grade were used. The absorption spectra of thin films were also measured in the glovebox using fiber optics connected to the spectrophotometer. Steady-state PL spectra were recorded using a PerkinElmer LS55 Fluorescence spectrophotometer. The PL quantum yield of the polymer in solution was calculated relative to the fluorescein or rhodamine 6G, which were used as standards.[77]

Electroluminescence Measurements. EL spectra were recorded using an Acton Research Spectrograph with single photon-counting detection (SPEX, RCA C31034 photomultiplier). LEDs were supplied from a Keysight Technologies B2901A Precision Source Measure Unit, which served to simultaneously record the current flowing through the sample. Current−voltage and luminance−voltage characteristics were recorded simultaneously using the source measure unit and a Minolta LS110 luminance meter or a silicon photodiode with integrated amplifier (EG&G HUV-4000B) for the detection of total light output. A voltage signal from the photodiode was recorded with a Hewlett-Packard 34401A multimeter. All measurements were conducted in a glovebox under a nitrogen atmosphere.

Photovoltaic Measurements. Current−voltage characteristics of the devices were recorded in the dark and under illumination (100 mW/cm^2) using a Keithley 2401 SourceMeter unit and a LS02821 LOT Quantum Design solar simulator. External quantum efficiencies (EQE) were measured with a setup consisting of EG&G Instruments 7260 DSP lock-in-amplifier, an optical chopper (SCITEC Instruments LTD), a xenon lamp LXH100 (Müller Elektronik-Optik), and a monochromator Acton Spectra Pro150. A calibrated silicon diode S2281 (Hamamatsu) was used as a reference.

■ ASSOCIATED CONTENT

Supporting Information

Supplementary data related to this article are available free of charge via the Internet at The Supporting Information is available free of charge on the ACS Publications website at DOI: 10.1021/acs.macromol.7b02136.

Synthesis of precursors, NMR and FTIR spectra, and thermo-gravimetric analysis plots (PDF)

■ AUTHOR INFORMATION

Corresponding Authors

*E-mail (V.C.): cimrova@imc.cas.cz or cimrova@gmail.com.
*E-mail (E.I.): eiwuoha@uwc.ac.za.
*E-mail (D.A.M.E.): daniel_ayuk_mbi.egbe@jku.at.

ORCID

Věra Cimrová: 0000-0001-5952-6320
Jean-François Morin: 0000-0002-9259-9051
Emmanuel Iwuoha: 0000-0001-6102-0433

Notes

The authors declare no competing financial interest.

■ ACKNOWLEDGMENTS

We thank the Czech Science Foundation (Grant 13-26542S), FWF (Project No. I 1703-N20) and the National Research Foundation (NRF) South African Agency for Science and Technology Advancement (Project No. UID-85102) for financial support. S.V.J. is grateful to the International Centre for Theoretical Physics (ICTP) and the African Network for Solar Energy (ANSOLE), as well as the NRF of South Africa, for financial support.

■ REFERENCES

(1) Schenning, A. P. H. J.; Meijer, E. W. Supramolecular electronics; nanowires from self-assembled π-conjugated systems. *Chem. Commun.* **2005**, 3245−3258.
(2) Hoeben, F. J. M.; Jonkheijm, P.; Meijer, E. W.; Schenning, A. P. H. J. About Supramolecular Assemblies of π-Conjugated Systems. *Chem. Rev.* **2005**, *105*, 1491−1546.
(3) Moulin, E.; Cid, J.-J.; Giuseppone, N. Advances in Supramolecular Electronics − From Randomly Self-assembled Nanostructures to Addressable Self-Organized Interconnects. *Adv. Mater.* **2013**, *25*, 477−487.
(4) Pisula, W.; Feng, X.; Müllen, K. Tuning the Columnar Organization of Discotic Polycyclic Aromatic Hydrocarbons. *Adv. Mater.* **2010**, *22*, 3634−3649.
(5) Zhang, L.; Walker, B.; Liu, F.; Colella, N. S.; Mannsfeld, S. C. B.; Watkins, J. J.; Nguyen, T.-Q.; Briseno, A. L. Triisopropylsilylethynyl-functionalized dibenzo[def,mno]chrysene: a solution-processed small molecule for bulk heterojunction solar cells. *J. Mater. Chem.* **2012**, *22*, 4266−4268.
(6) Mei, J.; Diao, Y.; Appleton, A. L.; Fang, L.; Bao, Z. Integrated Materials Design of Organic Semiconductors for Field-Effect Transistors. *J. Am. Chem. Soc.* **2013**, *135*, 6724−6746.
(7) Ye, Q.; Chi, C. Recent Highlights and Perspectives on Acene Based Molecules and Materials. *Chem. Mater.* **2014**, *26*, 4046−4056.
(8) Ball, M.; Zhong, Y.; Wu, Y.; Schenck, C.; Ng, F.; Steigerwald, M.; Xiao, S.; Nuckolls, C. Contorted Polycyclic Aromatics. *Acc. Chem. Res.* **2015**, *48*, 267−276.
(9) Collis, G. E. Designing small molecule polyaromatic p- and n-type semiconductor materials for organic electronics. *Proc. SPIE* **2015**, *9668*, 96683O−96683O-10.
(10) Schmidt-Mende, L.; Fechtenkotter, A.; Müllen, K.; Moons, E.; Friend, R. H.; MacKenzie, J. D. Self-Organized Discotic Liquid Crystals for High-Efficiency Organic Photovoltaics. *Science* **2001**, *293*, 1119−1122.
(11) Laschat, S.; Baro, A.; Steinke, N.; Giesselmann, F.; Hagele, C.; Scalia, G.; Judele, R.; Kapatsina, E.; Sauer, S.; Schreivogel, A.; Tosoni, M. Discotic Liquid Crystals: From Tailor-Made Synthesis to Plastic Electronics. *Angew. Chem., Int. Ed.* **2007**, *46*, 4832−4887.
(12) Wong, W. W. H.; Singh, T. B.; Vak, D.; Pisula, W.; Yan, C.; Feng, X.; Williams, E. L.; Chan, K. L.; Mao, Q.; Jones, D. J.; Ma, C.-Q.; Müllen, K.; Bäuerle, P.; Holmes, A. B. Solution Processable Fluorenyl Hexa-peri-hexabenzocoronenes in Organic Field-Effect Transistors and Solar Cells. *Adv. Funct. Mater.* **2010**, *20*, 927−938.
(13) Pisula, W.; Feng, X.; Müllen, K. Charge-Carrier Transporting Graphene-Type Molecules. *Chem. Mater.* **2011**, *23*, 554−567.
(14) Zhang, Z.; Lei, T.; Yan, Q.; Pei, J.; Zhao, D. Electron-transporting PAHs with dual perylenediimides: syntheses and semiconductive characterizations. *Chem. Commun.* **2013**, *49*, 2882−2884.
(15) Xiao, S.; Kang, S. J.; Zhang, S.; Scott, A. M.; Moscatelli, A.; Turro, N. J.; Steigerwald, M. L.; Li, H.; Nuckolls, C.; et al. Controlled Doping in Thin-Film Transistors of Large Contorted Aromatic Compounds. *Angew. Chem., Int. Ed.* **2013**, *52*, 4558−4562.
(16) He, B.; Tian, H.; Geng, Y.; Wang, F.; Müllen, K. Facile Synthesis of 9,10-Diarylphenanthrenes and Poly(9,10-diarylphenanthrene)s. *Org. Lett.* **2008**, *10*, 773−776.
(17) Kawano, S.-I.; Yang, C.; Ribas, M.; Baluschev, S.; Baumgarten, M.; Müllen, K. Blue-Emitting Poly(2,7-pyrenylene)s: Synthesis and Optical Properties. *Macromolecules* **2008**, *41*, 7933−7937.
(18) Saleh, M.; Park, Y.-S.; Baumgarten, M.; Kim, J.-J.; Müllen, K. Conjugated Triphenylene Polymers for Blue OLED Devices. *Macromol. Rapid Commun.* **2009**, *30*, 1279−1283.
(19) Chen, H.; Hu, X.; Ng, S.-C. Synthesis and characterization of soluble conjugated polymers having pyrene moiety in the main chain. *J. Polym. Sci., Part A: Polym. Chem.* **2010**, *48*, 5562−5569.
(20) Chou, C.-E.; Wang, D.; Bagui, M.; Hsu, J.; Chakraborty, S.; Peng, Z. Syntheses and optical properties of triphenylene-containing conjugated polymers. *J. Lumin.* **2010**, *130*, 986−994.

DOI: 10.1021/acs.macromol.7b02136
Macromolecules 2017, 50, 8357−8371

(21) Lehnherr, D.; Tykwinski, R. R. Conjugated Oligomers and Polymers Based on Anthracene, Tetracene, Pentacene, Naphthodithiophene, and Anthradithiophene Building Blocks. *Aust. J. Chem.* **2011**, *64*, 919−929.
(22) Kim, H.; Schulte, N.; Zhou, G.; Müllen, K.; Laquai, F. A High Gain and High Charge Carrier Mobility Indenofluorene-Phenanthrene Copolymer for Light Amplification and Organic Lasing. *Adv. Mater.* **2011**, *23*, 894−897.
(23) Yang, D. S.; Kim, K. H.; Cho, M. J.; Jin, J.-I.; Choi, D. H. Donor−acceptor alternating π-conjugated polymers containing Di(thiophen-2-yl)pyrene and 2,5-Bis(2-octyldodecyl)pyrrolo[3,4-c]-pyrrole-1,4(2H,5H)-dione for organic thin-film transistors. *J. Polym. Sci., Part A: Polym. Chem.* **2013**, *51*, 1457−1467.
(24) Li, G.; Kang, C.; Li, C.; Lu, Z.; Zhang, J.; Gong, X.; Zhao, G.; Dong, H.; Hu, W.; Bo, Z. Planar Conjugated Polymers Containing 9,10-Disubstituted Phenanthrene Units for Efficient Polymer Solar Cells. *Macromol. Rapid Commun.* **2014**, *35*, 1142−1147.
(25) Grimsdale, A. C.; Müllen, K. The Chemistry of Organic Nanomaterials. *Angew. Chem., Int. Ed.* **2005**, *44*, 5592−5629.
(26) Sun, Z.; Ye, Q.; Chi, C.; Wu, J. Low band gap polycyclic hydrocarbons: from closed-shell near infrared dyes and semiconductors to open-shell radicals. *Chem. Soc. Rev.* **2012**, *41*, 7857−7889.
(27) Hinkel, K.; Cho, D.; Pisula, W.; Baumgarten, M.; Müllen, K. Alternating Donor−Acceptor Arrays from Hexa-peri-hexabenzocoronene and Benzothiadiazole: Synthesis, Optical Properties, and Self-Assembly. *Chem. - Eur. J.* **2015**, *21*, 86−90.
(28) Giguère, J.-B.; Sariciftci, N. S.; Morin, J.-F. Polycyclic anthanthrene small molecules: semiconductors for organic field-effect transistors and solar cells applications. *J. Mater. Chem. C* **2015**, *3*, 601−606.
(29) Lafleur-Lambert, A.; Giguère, J.-B.; Morin, J.-F. Anthanthrene as a large PAH building block for the synthesis of conjugated polymers. *Polym. Chem.* **2015**, *6*, 4859−4863.
(30) Lafleur-Lambert, A.; Giguère, J.-B.; Morin, J.-F. Conjugated Polymers Based on 4,10-Bis(thiophen-2-yl)anthanthrone: Synthesis, Characterization, and Fluoride-Promoted Photoinduced Electron Transfer. *Macromolecules* **2015**, *48*, 8376−8381.
(31) Egbe, D. A. M.; Carbonnier, B.; Birckner, E.; Grummt, U.-W. Arylene-ethynylene/arylene-vinylene copolymers: Synthesis and structure−property relationships. *Prog. Polym. Sci.* **2009**, *34*, 1023−1067.
(32) Egbe, D. A. M.; Turk, S.; Rathgeber, S.; Kuhnlenz, F.; Jadhav, R.; Wild, A.; Birckner, E.; Adam, G.; Pivrikas, A.; Cimrova, V.; Knor, G.; Sariciftci, N. S.; Hoppe, H. Anthracene Based Conjugated Polymers: Correlation between π−π-Stacking Ability, Photophysical Properties, Charge Carrier Mobility, and Photovoltaic Performance. *Macromolecules* **2010**, *43*, 1261−1269.
(33) Günes, S.; Wild, A.; Cevik, E.; Pivrikas, A.; Schubert, U. S.; Egbe, D. A. M. Effect of shifting of aromatic rings on charge carrier mobility and photovoltaic response of anthracene and thiophene-containing MEH-PPE-PPVs. *Sol. Energy Mater. Sol. Cells* **2010**, *94*, 484−491.
(34) Susarova, D. K.; Khakina, E. A.; Troshin, P. A.; Goryachev, A. E.; Sariciftci, N. S.; Razumov, V. F.; Egbe, D. A. M. Photovoltaic performance of PPE-PPV copolymers: effect of the fullerene component. *J. Mater. Chem.* **2011**, *21*, 2356−2361.
(35) Tore, N.; Parlak, E. A.; Usluer, Ö.; Egbe, D. A. M.; San, S. E.; Aydogan, P. Effect of blend ratio on poly(p-phenylene-ethynylene)-alt-poly(p-phenylene-vinylene) polymer solar cells. *Sol. Energy Mater. Sol. Cells* **2012**, *104*, 39−44.
(36) Kästner, C.; Susarova, D. K.; Jadhav, R.; Ulbricht, C.; Egbe, D. A. M.; Rathgeber, S.; Troshin, P. A.; Hoppe, H. Morphology evaluation of a polymer−fullerene bulk heterojunction ensemble generated by the fullerene derivatization. *J. Mater. Chem.* **2012**, *22*, 15987−15997.
(37) Troshin, P. A.; Mukhacheva, O. A.; Usluer, Ö.; Goryachev, A. E.; Akkuratov, A. V.; Susarova, D. K.; Dremova, N. N.; Rathgeber, S.; Sariciftci, N. S.; Razumov, V. F.; Egbe, D. A. M. Improved Photovoltaic Performance of PPV-Based Copolymers Using Optimized Fullerene-Based Counterparts. *Adv. Energy Mater.* **2013**, *3*, 161−166.
(38) Saidani, M. A.; Benfredj, A.; Ben Hamed, Z.; Romdhane, S.; Ulbricht, C.; Egbe, D. A. M.; Bouchriha, H. Franck-Condon analysis of the photoluminescence spectra of a triple-bond containing polymer as a solution and as a thin film. *Synth. Met.* **2013**, *184*, 83−85.
(39) Gasiorowski, J.; Boudiba, S.; Hingerl, K.; Ulbricht, C.; Fattori, V.; Tinti, F.; Camaioni, N.; Menon, R.; Schlager, S.; Boudida, L.; Sariciftci, N. S.; Egbe, D. A. M. Anthracene-containing conjugated polymer showing four optical transitions upon doping: A spectroscopic study. *J. Polym. Sci., Part B: Polym. Phys.* **2014**, *52*, 338−346.
(40) Kösemen, A.; Tore, N.; Parlak, E. A.; Alpaslan Kösemen, Z.; Ulbricht, C.; Usluer, Ö.; Egbe, D. A. M.; Yerli, Y.; San, S. E. An efficient organic inverted solar cell with AnE-PVstat:PCBM active layer and V2O5/Al anode layer. *Sol. Energy* **2014**, *99*, 88−94.
(41) Kästner, C.; Egbe, D. A. M.; Hoppe, H. Polymer aggregation control in polymer−fullerene bulk heterojunctions adapted from solution. *J. Mater. Chem. A* **2015**, *3*, 395−403.
(42) Ding, L.; Egbe, D. A. M.; Karasz, F. E. Photophysical and Optoelectronic Properties of Green-Emitting Alkoxy-Substituted PE/PV Hybrid Conjugated Polymers. *Macromolecules* **2004**, *37*, 6124−6131.
(43) Egbe, D. A. M.; Nguyen, L. H.; Carbonnier, B.; Mühlbacher, D.; Sariciftci, N. S. Thiophene-containing poly(arylene−ethynylene)-alt-poly(arylene−vinylene)s: Synthesis, characterisation and optical properties. *Polymer* **2005**, *46*, 9585−9595.
(44) Wild, A.; Egbe, D. A. M.; Birckner, E.; Cimrova, V.; Baumann, R.; Grummt, U.-W.; Schubert, U. S. Anthracene- and thiophene-containing MEH-PPE-PPVs: Synthesis and study of the effect of the aromatic ring position on the photophysical and electrochemical properties. *J. Polym. Sci., Part A: Polym. Chem.* **2009**, *47*, 2243−2261.
(45) Usluer, Ö.; Kästner, C.; Abbas, M.; Ulbricht, C.; Cimrova, V.; Wild, A.; Birckner, E.; Tekin, N.; Sariciftci, N. S.; Hoppe, H.; Rathgeber, S.; Egbe, D. A. M. Charge carrier mobility, photovoltaic, and electroluminescent properties of anthracene-based conjugated polymers bearing randomly distributed side chains. *J. Polym. Sci., Part A: Polym. Chem.* **2012**, *50*, 3425−3436.
(46) Egbe, D. A. M.; Roll, C. P.; Klemm, E. Synthesis, characterisation and properties of highly luminescent and liquid-crystalline alternating PPE/PPV-copolymers. *Des. Monomers Polym.* **2002**, *5*, 245−275.
(47) Egbe, D. A. M.; Roll, C. P.; Birckner, E.; Grummt, U.-W.; Stockmann, R.; Klemm, E. Side Chain Effects in Hybrid PPV/PPE Polymers. *Macromolecules* **2002**, *35*, 3825−3837.
(48) Egbe, D. A. M.; Carbonnier, B.; Ding, L.; Mühlbacher, D.; Birckner, E.; Pakula, T.; Karasz, F. E.; Grummt, U.-W. Supramolecular Ordering, Thermal Behavior, and Photophysical, Electrochemical, and Electroluminescent Properties of Alkoxy-Substituted Yne-Containing Poly(phenylene−vinylene)s. *Macromolecules* **2004**, *37*, 7451−7463.
(49) Egbe, D. A. M.; Sell, S.; Ulbricht, C.; Birckner, E.; Grummt, U.-W. Mixed Alkyl- and Alkoxy-Substituted Poly[(phenylene ethynylene)-alt-(phenylene vinylene)] Hybrid Polymers: Synthesis and Photophysical Properties. *Macromol. Chem. Phys.* **2004**, *205*, 2105−2115.
(50) Egbe, D. A. M.; Carbonnier, B.; Paul, E. L.; Muhlbacher, D.; Kietzke, T.; Birckner, E.; Neher, D.; Grummt, U.-W.; Pakula, T. Diyne-Containing PPVs: Solid-State Properties and Comparison of Their Photophysical and Electrochemical Properties with Those of Their Yne-Containing Counterparts. *Macromolecules* **2005**, *38*, 6269−6275.
(51) Giguere, J. B.; Boismenu-Lavoie, J.; Morin, J. F. Cruciform Alkynylated Anthanthrene Derivatives: A Structure-Properties Relationship Case Study. *J. Org. Chem.* **2014**, *79*, 2404−2418.
(52) Osuna, R. M.; Zhang, X.; Matzger, A. J.; Hernandez, V.; Lopez Navarrete, J. T. Combined Quantum Chemical Density Functional Theory and Spectroscopic Raman and UV−vis−NIR Study of Oligothienoacenes with Five and Seven Rings. *J. Phys. Chem. A* **2006**, *110*, 5058−5065.

DOI: 10.1021/acs.macromol.7b02136
Macromolecules 2017, 50, 8357−8371

(53) Zheng, C.; Tao, Y.; Cao, J.-Z.; Chen, R.-F.; Zhao, P.; Wu, X.-J.; Huang, W. The structural, electronic, and optical properties of ladder-type polyheterofluorenes: a theoretical study. *J. Mol. Model.* **2012**, *18*, 4929−4939.
(54) Sghaier, T.; Le Liepvre, S.; Fiorini, C.; Douillard, L.; Charra, F. Optical absorption signature of a self-assembled dye monolayer on graphene. *Beilstein J. Nanotechnol.* **2016**, *7*, 862−868.
(55) Cimrová, V.; Neher, D.; Remmers, M.; Kmínek, I. Blue Light-Emitting Devices Based on Novel Polymer Blends. *Adv. Mater.* **1998**, *10*, 676−680.
(56) Cimrová, V.; Výprachtický, D.; Hoerhold, H.-H. Poly[methyl-(phenyl)silanediyl] Modified with Dansyl Fluorophore: Synthesis and Photophysics. *J. Polym. Sci., Part A: Polym. Chem.* **2011**, *49*, 2233−2244.
(57) Cimrová, V.; Výprachtický, D. Enhanced Electroluminescence from Light-Emitting Devices Based on Poly(9,9-dihexadecylfluorene-2,7-diyl) and Polysilane Blends. *Appl. Phys. Lett.* **2003**, *82*, 642−644.
(58) Cimrová, V.; Výprachtický, D. Electroluminescence and charge photogeneration in poly(9,9-dihexadecylfluorene-2,7-diyl) and its blends. *Macromol. Symp.* **2004**, *212*, 281−286.
(59) Mikroyannidis, J. A.; Barberis, V. P.; Výprachtický, D.; Cimrová, V. Simple Synthesis, Photophysics and Electroluminescent Properties of Poly[2,7-bis(4-tert-butylstyryl)fluorene-9,9-diyl-alt-alkane-α,ω-diyl]. *J. Polym. Sci., Part A: Polym. Chem.* **2007**, *45*, 809−821.
(60) Chen, S.-H.; Li, Y.-R.; Yu, Ch.-F.; Lin, Ch.-F.; Kao, P.-Ch. Enhanced luminescence efficiency of Ag nanoparticles dispersed on indium tin oxide for polymer light-emitting diodes. *Opt. Express* **2013**, *21*, 26236−26243.
(61) Chen, Y.; Smith, G. M.; Loughman, E.; Li, Y.; Nie, W.; Carroll, D. L. Effect of multi-walled carbon nanotubes on electron injection and charge generation in AC field-induced polymer electroluminescence. *Org. Electron.* **2013**, *14*, 8−18.
(62) Ying, L.; Ho, Ch.−L.; Wu, H.; Cao, Y.; Wong, W.-Y. White Polymer Light-Emitting Devices for Solid-State Lighting: Materials, Devices, and Recent Progress. *Adv. Mater.* **2014**, *26*, 2459−2473.
(63) Beaujuge, P. M.; Fréchet, J. M. J. Molecular Design and Ordering Effects in π-Functional Materials for Transistor and Solar Cell Applications. *J. Am. Chem. Soc.* **2011**, *133*, 20009−20029.
(64) Scharber, M. C.; Sariciftci, N. S. Efficiency of bulk-heterojunction organic solar cells. *Prog. Polym. Sci.* **2013**, *38*, 1929−1940.
(65) Choi, H.; Kim, H.-B.; Ko, S.-J.; Kim, J. Y.; Heeger, A. J. An organic surface modifier to produce a high work function transparent electrode for high performance polymer solar cells. *Adv. Mater.* **2015**, *27*, 892−896.
(66) Choi, H.; Ko, S.-J.; Kim, T.; Morin, P.-O.; Walker, B.; Lee, B. H.; Leclerc, M.; Kim, J. Y.; Heeger, A. J. Small-bandgap polymer solar cells with unprecedented short-circuit current density and high fill factor. *Adv. Mater.* **2015**, *27*, 3318−3324.
(67) Vohra, V.; Kawashima, K.; Kakara, T.; Koganezawa, T.; Osaka, I.; Takimiya, K.; Murata, H. Efficient inverted polymer solar cells employing favourable molecular orientation. *Nat. Photonics* **2015**, *9*, 403−408.
(68) Yuan, J.; Ouyang, J.; Cimrová, V.; Leclerc, M.; Najari, A.; Zou, Y. Development of quinoxaline based polymers for photovoltaic applications. *J. Mater. Chem. C* **2017**, *5*, 1858−1879.
(69) Cimrová, V.; Morávková, Z.; Pokorná, V.; Výprachtický, D. Investigation of donor−acceptor copolymer films and their blends with fullerene in the active layers of bulk heterojunction solar cells by Raman microspectroscopy. *Org. Electron.* **2017**, *47*, 194−199.
(70) Liu, Y.; Mu, C.; Jiang, K.; Zhao, J.; Li, Y.; Zhang, L.; Li, Z.; Lai, J. Y. L.; Hu, H.; Ma, T.; Hu, R.; Yu, D.; Huang, X.; Tang, B. Z.; Yan, H. A tetraphenylethylene core-based 3D structure small molecular acceptor enabling efficient non-fullerene organic solar cells. *Adv. Mater.* **2015**, *27*, 1015−1020.
(71) Li, S.; Liu, W.; Shi, M.; Mai, J.; Lau, T.-K.; Wan, J.; Lu, X.; Li, C.-Z.; Chen, H. A spirobifluorene and diketopyrrolopyrrole moieties based non-fullerene acceptor for efficient and thermally stable polymer solar cells with high open-circuit voltage. *Energy Environ. Sci.* **2016**, *9*, 604−610.
(72) Li, Y.; Liu, X.; Wu, F.-P.; Zhou, Y.; Jiang, Z.-Q.; Song, B.; Xia, Y.; Zhang, Z.-G.; Gao, F.; Inganäs, O.; Li, Y.; Liao, L.-S. Non-fullerene acceptor with low energy loss and high external quantum efficiency: towards high performance polymer solar cells. *J. Mater. Chem. A* **2016**, *4*, 5890−5897.
(73) Yuan, J.; Qiu, L.; Zhang, Z.-G.; Li, Y.; Chen, Y.; Zou, Y. Tetrafluoroquinoxaline based polymers for non-fullerene polymer solar cells with efficiency over 9%. *Nano Energy* **2016**, *30*, 312−320.
(74) Yuan, J.; Qiu, L.; Zhang, Z.; Li, Y.; He, Y.; Jiang, L.; Zou, Y. A simple strategy to the side chain functionalization on the quinoxaline unit for efficient polymer solar cells. *Chem. Commun.* **2016**, *52*, 6881−6884.
(75) Zhang, Z.; Feng, L.; Xu, S.; Yuan, J.; Zhang, Z.-G.; Peng, H.; Li, Y.; Zou, Y. Achieving over 10% efficiency in a new acceptor ITTC and its blends with hexafluoroquinoxaline based polymers. *J. Mater. Chem. A* **2017**, *5*, 11286−11293.
(76) Chen, W.; Zhang, Q. Recent progress in non-fullerene small molecule acceptors in organic solar cells (OSCs). *J. Mater. Chem. C* **2017**, *5*, 1275−1302.
(77) Brouwer, A. M. Standards for photoluminescence quantum yield measurements in solution (IUPAC Technical Report). *Pure Appl. Chem.* **2011**, *83*, 2213−2228.

DOI: 10.1021/acs.macromol.7b02136
Macromolecules 2017, 50, 8357−8371